ANL/NEAMS-24/3

Assessment and validation of NEAMS tools for high-fidelity multiphysics transient modeling of microreactors

Application of NEAMS codes to perform multiphysics modeling analyses of micro-reactor concepts

Nuclear Science and Engineering Division

About Argonne National Laboratory

Argonne is a U.S. Department of Energy laboratory managed by UChicago Argonne, LLC under contract DE-AC02-06CH11357. The Laboratory's main facility is outside Chicago, at 9700 South Cass Avenue, Argonne, Illinois 60439. For information about Argonne and its pioneering science and technology programs, see www.anl.gov.

ANL/NEAMS-24/3

Assessment and validation of NEAMS tools for high-fidelity multiphysics transient modeling of microreactors

Application of NEAMS codes to perform multiphysics modeling analyses of micro-reactor concepts

prepared by
N. Stauff, A. Abdelhameed, Y. Cao, L. Ibarra, S. K. Lee, Y. Miao, K. Mo
Argonne National Laboratory

September 30, 2024

EXECUTIVE ABSTRACT

The NEAMS Multiphysics Applications team aims at providing assessment of code useability and functionality for microreactor design and analyses, together with demonstration of their capabilities to properly capture the steady-state and time-dependent behavior of different microreactor concepts. In FY-2024, significant progress was achieved in improving multi-physics models of several microreactors systems: HP-MR, GC-MR and KRUSTY. These efforts focused on solving more complex multiphysics problems enabled by enhanced tools capability, verifying and validating results obtained, providing feedback to developers for suggested improvements, and sharing these models to facilitate user training.

A series of new multiphysics transients were completed on the HP-MR (using Griffin/BISON/Sockeye) with core startup transient, control drum inadvertent rotation accident, and hydrogen leakage from hydride moderator (also including SWIFT). On the GC-MR, a new full-core model was developed and analyzed through a series of new multiphysics (Griffin/BISON/SAM) transients to simulate moderator leakage (also including SWIFT), flow blockage and coolant depressurization.

Additional and updated TRISO failure analyses were completed on the HP-MR unit-cell and GC-MR assembly models leveraging improved TRISO modeling capabilities. The amount of SiC failure following accidental transients at end-of-life was null. However, GC-MR assembly TRISO analysis highlighted Pd penetration rate can be problematic and may require design changes on the studied microreactor concept.

The neutronics discrepancies observed on the KRUSTY model in previous years were resolved using hybrid set of Monte Carlo/Deterministic cross-sections. The multiphysics (Griffin neutronics / BISON thermal-mechanics) 15¢ insertion transient simulation displayed good agreement when comparing with experimental data. Initial modeling of the 30 ¢ reactivity insertion also displays promising results. Such close agreement provides important validation data that can be leveraged by the NEAMS program and by microreactor vendors to support licensing of their technology.

Finally, important experience was gathered with the NEAMS tools leading to several user feedback shared with tools developers, especially with regards to MOOSE mesh generator and Griffin. This project led to many publications demonstrating modeling capabilities, and to three models shared on the Virtual Test Bed.

ACKNOWLEDGEMENTS

This work was supported by the Department of Energy – Nuclear Energy Advanced Modeling and Simulation Program (NEAMS) under the Multiphysics Applications Technical Area.

The team would like to express appreciation to Emily Shemon, Cody Permann, and Christopher Matthews for their reviews and support throughout this project.

Invaluable support was provided by the Sockeye developers (Joshua Hansel, Elia Merzari, and Lise Charlot), Griffin developers (Changho Lee, Javier Ortensi, Yaqi Wang, Yeon Sang Jung, Prince Zachary, Vincent M. Laboure), Reactor module and MeshGenerator system developers (Emily Shemon, Shikhar Kumar, Yeon Sang Jung, Aaron Oaks), BISON developers (Wen Jiang, Stephen Novascone, Jacob Hirschhorn), and SWIFT developer (Christopher Matthews), MOOSE framework developers (Logan Harbour, Guillaume Giudicelli, Alexander Lindsay).

The VTB reviews from Guillaume Giudicelli were instrumental in providing directions for improvements of submitted models. Special thanks to Wen Jiang for invaluable discussions and support in the TRISO analysis and review.

This research made use of Idaho National Laboratory computing resources which are supported by the Office of Nuclear Energy of the U.S. Department of Energy and the Nuclear Science User Facilities under Contract No. DE-AC07-05ID14517.

TABLE OF CONTENTS

LIST OF FIGURES

LIST OF TABLES

1 Introduction

The U.S. Department of Energy (DOE) Office of Nuclear Energy's Advanced Modeling and Simulation (NEAMS) program [1] is actively developing advanced modeling tools to support core design and safety analyses of advanced nuclear reactors. In particular, micro-nuclear reactors employ innovative features such as heat pipes or hydride moderator modules, non-traditional geometries such as control drums, and have flexible operation requirements. All these microreactor-specific characteristics prevent reactor vendors from using traditional commercial tools for modeling. The NEAMS program aims to provide high-fidelity multiphysics modeling capabilities to support design and licensing of various types of advanced nuclear reactors, including the technologies being developed by U.S. microreactor vendors. Within this program, the Multiphysics Applications team provides assessment of code useability and functionality for microreactor design and analyses, together with demonstration of their capabilities to properly capture the steady-state and time-dependent behavior of different microreactor concepts.

This project builds on years of expertise acquired by different teams and programs [2] [3] [4]. In previous work completed in FY-2023 [5], detailed high-fidelity multiphysics modeling of a wide range of transient scenarios were completed for full cores heat pipe (HP-MR) and gas-cooled (GC-MR) microreactors. In addition, a detailed model for the Kilopower Reactor Using Stirling Technology (KRUSTY) experiment was developed.

This report summarizes the work done by the NEAMS Multiphysics Applications Microreactor team in FY-2024. First, the user's assessment of NEAMS tools (MOOSE Mesh generator, Multiapp, BISON, Griffin, SAM, Sockeye and SWIFT) used in this project is summarized in Section 2. The HP-MR analysis was further improved through high-fidelity Multiphysics modeling of new transients and physics phenomena (core startup, hydrogen leakage from moderator, control drums inadvertent rotation, TRISO failure) as reported in Section 3. Similar new transients were also applied on a new full-core GC-MR model, as reported in Section 4. Major effort was completed on KRUSTY to resolve some of the remaining discrepancies observed in FY-2023 and support validation of multiphysic simulations through modeling several experimental reactivity insertion transients, as reported in Section 5. Finally, the work completed is summarized in Section 6, highlighting lessons learned for microreactor modelers and for NEAMS developers.

2 Method Description and Assessment

This section summarizes the different NEAMS capabilities applied in this project with a focus on the new or existing modules that were assessed in FY-2023 as summarized in Table 2-1. The codes considered for microreactor modeling include Griffin [6] for neutronics, BISON [7] for thermo-mechanics, Sockeye [8] for heat pipe modeling, SAM [9] for 1D flow modeling across the coolant channels, and SWIFT [10] for hydrogen redistribution modeling. All the codes are developed within the MOOSE framework to facilitate multiphysics coupling with the MultiApp system [11]. The meshes are developed with the MOOSE Reactor Module [12] and related MeshGenerator objects. Some results of our assessment are summarized in this section, including the list of development requests and user feedback made to the different code developers.

Table 2-1. Summary of codes and module assessed in FY-2023.

Code	**Module Assessed or Capability used**	**Applied Section**
MOOSE Mesh System	Various mesh generators were used for 3-D modeling of inadvertent control drum rotation such as: *HexagonConcentricCircleAdaptiveBoundaryMeshGenerator* *AzimuthalBlockSplitGenerator* *PatternedHexPeripheralModifier* *AdvancedExtruderGenerator*	3.4.1
Griffin	DFEM-SN and CMFD for acceleration MC^2-3 cross-section used in Griffin	3.1, 4.2, 5.1.3 5.1.2
BISON	Solid Mechanics, Stochastic Module, Latest SiC mechanical, Pd penetration, and failure models for TRISO particle analysis	3.5, 4.3, 4.4
SWIFT	Hydrogen redistribution and leaking under different scenarios	3.2, 4.3.3
Sockeye	Vapor-Only model: one-dimensional, compressible flow equations for the vapor phase and two-dimensional heat conduction equation for the wick, liquid and cladding.	3.3
SAM	Same as FY-2023	4
MultiApp	Distributed mesh approach along with mesh pre-splitting	3, 4.3, 5.2

2.1 MeshGenerator

The MOOSE Reactor Module [12] was employed to generate 3D meshes for whole core HP-MR and GC-MR. This FY, a new full-core mesh was created for the GC-MR, as described in Section 4.2. For its pin design, the *PolygonConcentricCircleMeshGenerator* was used, which is effective for creating 2D meshes with concentric circles within a polygonal boundary. This approach is suited for pin cell geometries where distinct mesh densities are required for regions such as fuel, cladding,

and moderator. Following this, the *PatternedHexMeshGenerator* was utilized to apply hexagonal patterns across complex core layouts. This generator is facilitating multi-region meshes and assigning block IDs and names.

For HP-MR control drum rotation modeling described in Section 3.4, different mesh options were tested. Two models were considered for steady-state code-to-code verification. In the first model, the poison region is explicitly modeled within the mesh, while in the second model, the poison and non-poison regions in the drums are treated as a single block. For the transient accidental control drum scenario, the mesh model was optimized to ensure fine discretization in the control drum region while maintaining a reasonable overall mesh size. This was achieved by using coarser elements in the core region to balance accuracy and computational efficiency. To enable finer discretization in the control drum region, the *PatternedHexPeripheralModifier* was applied. This tool adjusts assembly boundaries, ensuring seamless stitching of different assemblies within the reactor core while maintaining consistent node counts across boundaries. The *HexagonConcentricCircleAdaptiveBoundaryMeshGenerator* proved to be valuable in the modeling of control drums, allowing for boundary adjustments within a hexagonal mesh. This capability is useful for refining specific areas, like control drums, without impacting the entire model. Additionally, the *AzimuthalBlockSplitGenerator* was employed to specify the positions of blocks within the drum by defining start and end angles, thereby facilitating the creation of rotational elements necessary for simulating control drum movements. Dummy assemblies were also efficiently generated and defined using the *HexagonConcentricCircleAdaptiveBoundaryMeshGenerator*, and unnecessary blocks were removed using the *BlockDeletionGenerator*. The *AdvancedExtruderGenerator* was effective in addressing complex modeling requirements for the microreactor core, such as different fuel assembly designs, unique axial loading configurations for burnable absorbers, and the intricate design of control drums. Transitioning the mesh from a 2D to a 3D structure, and incorporating distinct axial regions, was straightforward. This generator facilitates the establishment of varying heights for different elevations, supports the definition of multiple layers within each elevation, allows for adjustable growth factors in axial element dimensions, and enables the remapping of subdomain IDs, boundary IDs, and other integer attributes within each elevation.

Suggestions: In the current HP-MR model, 12 separate blocks are required to model control drums, each with identical ring_radii and hexagon_size inputs, differing only in sides_to_adapt and ring_block_ids. By allowing users to define shared parameters like ring_radii and hexagon_size once, while specifying only the unique parameters for each drum, the process could be made more efficient. This approach could also streamline the configuration of reflector blocks. Additionally, another 12 separate blocks are needed to define each drum's start and end angles using the *AzimuthalBlockSplitGenerator*. An improvement would be to automate the definition of these angles based on a global control drum status. For example, introducing an option that allows users to set the status of all control drums with a single command (e.g., control_drums=0 to indicate all drums are inserted, or control_drums=180 for fully rotated out) would simplify the process.

2.2 Griffin and cross section generations using MC^2-3 and Serpent-2

Griffin [6] is a Finite Element (FE) neutronic code that can solve steady-state, transient or eigenvalue transport problems on both conventional and unconventional geometries such as those found in HP-MR, GC-MR and KRUSTY microreactor designs analyzed in this report. It takes

multigroup cross sections in the ISOXML format and has different numerical solvers equipped to solve the different neutronic problems.

In this project, the DFEM-SN discretization scheme together with the SweepUpdate executioner and the CMFD acceleration scheme are the main tools used to discretize and solve the multigroup neutron transport problems. The neutron multigroup cross sections were generated from Serpent-2 Monte Carlo simulations [13]. For KRUSTY, the reactor lattice physics code MC^2-3 was also used for preparing zone homogenized macroscopic cross sections [14].

Our analyses on using Griffin for neutronic calculations of the HP-MR (Section 3.1), GC-MR (Section 4.2) and KRUSTY (Section 5.1.3) show that Griffin can provide transport solutions with reasonable agreement to the solutions obtained from the continuous energy Monte Carlo code Serpent-2. However, there are also lessons learned from our modeling exercises that are documented here.

First, two main lessons were learned on using Serpent-2 to generate cross sections for modeling KRUSTY:

- The cross sections generated from the Monte Carlo method can lead to larger biases in calculating the core criticality of a fast spectrum small leaky core such as KRUSTY when the anisotropic scattering is important. The ANL lattice physics code MC^2-3 for fast reactors provides better high-order anisotropic cross sections in the reflector region but fails to predict an accurate fuel Doppler reactivity feedback. A hybrid cross section set which combines cross sections from MC^2-3 in the reflector region and cross sections from Serpent-2 in all other regions is a workaround solution for KRUSTY. But due to the limitation on the current version in MC^2-3, the cross sections were generated using ENDF/B-VII.0 library instead of using the most recent ENDF/B-VIII.0 library.
- In Serpent-2 simulation, it is important to provide an intermediate energy group structure to obtain better diffusion coefficients. This energy group structure must be finer than the energy grid used for condensing broad energy group cross sections. Simulations performed on KRUSTY showed that using an intermediate energy group structure the same as the broad energy group structure leads to wrong k-eff prediction from the Griffin calculation.

For coupling the neutronics calculation with other physics codes like BISON, the current process of creating tabulated cross-sections across different grids is cumbersome and requires user-scripting to automate this process. Currently, a separate Serpent-2 input at each grid point needs to be executed individually. The Serpent-2 output files need to be renamed in a specific sequence to convert them into the proper isoxml format. However, Serpent-2 now allows users to create branches and coefficient matrices to generate cross-sections at different temperatures and depletion points through a single execution. In the future, streamlining this ISOXML generation workflow using Serpent-2 branching calculation output would simplify the process of creating the multi-group cross-sections.

A saturation error was observed in some cases for GC-MR when using the DFEM-SN discretization scheme with the SweepUpdate executioner and using the CMFD for acceleration. The issue is found to be related to the coarse meshes used in specific large core regions such as shielding region. While smaller mesh elements can be a workaround, it is sometimes not possible to run the case with finer meshes in these large regions, especially considering that the current memory required by CMFD is relatively large. It would be highly beneficial if Griffin could automatically detect

saturation errors and stop the iteration with potential solutions suggested to the user to improve the convergence (such as refining mesh in some regions). It should be noted that using a coarser mesh with less accurate results can be useful for scoping analyses, when a higher accuracy is computationally expensive for analyses.

Given the relatively large memory requirements for DFEM-SN CMFD, we encounter issues of developing full core models that is necessary in the simulations. For instance, a full core model is needed in our GC-MR model when modeling the control drum rotations because Griffin's transport solver currently lacks support for rotational boundary conditions (as already highlighted in FY-2023 [5]). Rather we have only modeled a portion (e.g., 1/6 core) due to the limited memory resources on the cluster.

The treatment of the cusping effect is not yet fully developed in Griffin, which issue was encountered in the HP-MR control drum rotation modeling (Section 3.4). The cusping effect is anomaly in power distribution calculation arises due to discretization when the cross-sections of absorbing and non-absorbing materials clearly different. While it is possible to mitigate this effect by refining the mesh so that the front of the drum aligns with element edges at every time step. This refinement reduces flexibility in time step sizes and unnecessarily increases the number of elements and computational resources required.

Finally, the current Griffin only gives a one-time warning when the sampled grid variable value exceeds the range of that grid variable as defined in the cross section. It is recommended that a more prominent message can be thrown in such cases as Griffin does not extrapolate grid variables. This would be particularly useful for the transient simulations as the grid variables such as temperature could be dynamic in such types of simulations. This would be crucial to help users identify and investigate resulting non-physical results.

Addressing these issues would improve Griffin's usability and enhance further its modeling capability.

2.3 BISON

BISON [7] is a cutting-edge nuclear fuel performance code, developed within the Multiphysics Object-Oriented Simulation Environment (MOOSE) framework. Designed with versatility, BISON is capable of modeling a wide variety of fuel forms, such as light water reactor fuel rods, TRISO particle fuel, and metallic rod and plate fuel.

During FY-2024, BISON has continued to be adopted and assessed in two distinct capacities: (1) macroscopic full-core modeling of HP-MR, GC-MR, and KRUSTY, and (2) microscale TRISO fuel failure probability analysis. The use of BISON in these applications can be divided into two categories: heat transfer simulation and thermomechanical simulation.

For the full core simulations of HP-MR and GC-MR, BISON has been used only for thermal physics, namely, the heat conduction in the solid/static components of the microreactors. On the other hand, for the full core simulations of KRUSTY, as thermal expansion is crucial to this fast spectrum microreactors and the relative simplicity of its reactor design, thermomechanical simulations have been performed using BISON to not only predict the heat transfer but also the thermal expansion/thermal stress in KRUSTY.

For TRISO failure analysis, BISON’s thermomechanical capabilities were used for both assembly stress modeling as well as the detailed single particle modeling. The primary TRISO particle model

was refined based on the FY-2023 model. In a TRISO fuel, the monolithic silicon carbide (SiC) layer plays a crucial role as the primary structural and retention barrier for containing fission products. Major model updates were made to SiC layer to enhance its mechanical responses and improve the overall TRISO failure analysis during the steady-state fuel cycle of the HP-MR.

The TRISO model was updated with the latest SiC mechanical models to enhance TRISO stress evaluation during steady-state operations for both HP-MR and GC-MR. Irradiation-induced effects were accounted for using the *MonolithicSiCVolumetricSwellingEigenstrain* and *MonolithicSiCCreepUpdate* objects. Both models calculate SiC mechanical deformation using fast neutron fluence values supplied by the *FastNeutronFlux* object. While we leveraged the core-average fast neutron flux conversion factor from Serpent-2 analysis at the beginning-of-cycle, improved accuracy in stress analysis can be achieved by implementing locational fast neutron flux calculations from multiphysics analysis.

Furthermore, the TRISO analysis from the GC-MR highlighted potential palladium penetration-induced failure in the SiC layer during high-temperature operations. The current palladium penetration and failure threshold models are empirical and somewhat limited in scope. This underscores the need for a mechanistic palladium penetration model in BISON to accurately incorporate corrosion kinetics into SiC mechanical properties.

2.4 SWIFT

SWIFT is a MOOSE application dedicated to simulating the performance of hydride-based moderator. ANL received a license to SWIFT from LANL in mid-FY-2023 and then initiated the assessment efforts in FY-2023. In FY-2024, more extensive SWIFT-based hydride performance analyses were implemented into the full core GC-MR (in Section 4.3) and HP-MR models (in Section 3.2).

SWIFT usually uses a 2D-RZ mesh representing a column of hydride moderator pellets enclosed by a cladding material with hydrogen permeation barrier coating. The pellet-cladding gap and plenum are also meshed and simulated explicitly to account for hydrogen diffusion in gas. The hydrogen diffusion within the solid hydride as well as the surface reaction is also simulated. Based on the state of hydrogen gas, the permeation rate is also calculated so that the loss of hydrogen through the cladding/weld can be governed. The SWIFT code worked as expected and yielded reasonable results throughout this year's project. For GC-MR, a convergence issue was found when coupling SWIFT with other physical models (see Section 4.3), but this is likely coming from a coupling issue instead of a standalone SWIFT issue.

In FY-2024, more advanced features available in SWIFT have been utilized to evaluate the impact of hydride moderator performance on microreactor performance during normal operation and transient scenarios (see Sections 3.2 and 4.3). Various leakage mechanisms of the hydride moderator enclosure have been explored, including common permeation through cladding/welding, welding failure, and loss of the end cap. The leakage was found to result in significant alterations in hydrogen concentration, impacting reactivity.

One potential new feature that could benefit future microreactor simulations is the introduction of permeation barrier degradation models. For instance, alumina is a coating commonly applied to hydride moderator cladding to suppress hydrogen permeation [15]. It provides excellent hydrogen barrier performance with yttrium hydride below approximately 1000°C. However, as the operating temperature exceeds 1000°C, the elevated temperature and subsequent high hydrogen pressure

activate the reduction reaction between hydrogen gas and alumina, compromising the hydrogen barrier performance. Implementing such models into SWIFT could enhance future high-temperature modeling of hydride moderator modules.

Currently, SWIFT is manually distributed and lacks an official GitHub or GitLab repository, unlike the other MOOSE applications examined in this report. This limitation hinders the further development and promotion of the code. Establishing an official repository is essential for SWIFT to become a component of MOOSE super applications such as BlueCRAB and DireWolf, and to be included in models published in the Virtual Test Bed.

2.5 Sockeye

Sockeye is a MOOSE-based heat pipe simulator and analysis tool. Heat pipe simulation predicts heat transfer for heat pipe applications, including heat-pipe-cooled microreactors. Additionally, it provides insight into heat pipe performance; operational heat pipe limits can be predicted for transient conditions. Heat pipe simulation can be used by industry to inform heat pipe and microreactor design. Simulations can be performed to determine the range of operating conditions applied to a heat pipe and whether reliable heat pipe operation can be sustained in these conditions. If operational limits are encountered, heat pipe design can be altered to avoid these limits. Sockeye's primary focus is on liquid-metal pipes with annular screen or porous wick structures. Its intended application is the simulation of heat pipes in microreactors.

Sockeye can model the two-phase flow of the working fluid inside the heat pipe using a 1-D approximation. The code can perform these calculations for normal operation, startup, and shutdown conditions. This report documents the results of the vapor-only flow model testing for HP-MR, the development of a tutorial for this capability, and its application to a full-core HP-MR test case from the VTB, in Section 3.3.

In this model, a 1D single-phase, compressible flow formulation for the vapor phase in the core region is coupled to 2D heat conduction in the wick and annulus [16]. The coupling between the vapor core and wick is performed with interfacial heat and mass transfer terms. The liquid/solid working fluid inventory in the evaporator section is tracked with an ordinary differential equation. It depletes with evaporation, but while the heat pipe is within the capillary limit, it replenishes. This model currently assumes/requires a "standard" heat pipe configuration, i.e., the heat pipe has a single evaporator section and a single condenser section, optionally separated by an adiabatic section.

The following is a summary of Sockeye's capabilities:

- Transient, 1-D, two-phase flow coupled to 2-D heat conduction
- Transient, 2-D, effective thermal conductivity model
- Analytic tools for analyzing heat pipe operating envelope

Additional information on Sockeye is available in the Sockeye User's Manual [17]. Missing information on the model descriptions and input requirements during the preparation of the test cases and tutorials made the preparation of these test cases difficult. Gaps in the documentation are

known and current efforts are underway to bridge them. The publication of the vapor-only model was published in [16].

2.6 SAM

The System Analysis Module (SAM) [9] is a modern system analysis tool being developed by the NEAMS program for advanced non-LWR safety analysis. SAM is a MOOSE-based application, which allows for flexible coupling with other MOOSE-based applications. In addition, SAM has direct access to capabilities provided in MOOSE framework and its physics modules such as Navier-Stokes Module and Thermal Hydraulics Module (THM). The modeling of the whole core GC-MR was completed in section 4 using SAM, using similar approach and models as developed in FY-2023 [5].

2.7 MultiApp System

The NEAMS codes Griffin, SAM, Sockeye, SWIFT, and BISON were employed to carry out time-dependent simulations of the HP-MR (Section 3), GC-MR (Section 4.3), and KRUSTY (Section 5.2) models in both normal and accidental scenarios. Figure 2-1 illustrates the structure of the MOOSE MultiApp system typically employed in our analyses, with Griffin as the parent application. This MultiApp system [11] facilitated smooth data interchange between Griffin, its child application (BISON), and its grandchild applications (SAM, Sockeye, and SWIFT).

As a MOOSE application, SWIFT is capable of performing diffusion-based heat conduction simulations intrinsically to solve the temperature profile within the moderator module. However, since the moderator temperature has already been calculated in the BISON child application, the temperature profile of the SWIFT model is transferred from the BISON child application instead. The hydrogen distribution in moderator modules, as calculated by SWIFT, is transferred back to the BISON child application. The BISON child application collects the hydrogen distribution from different hydride moderator modules and then transfers the full-core hydrogen distribution information to the Griffin parent application, where the hydrogen information can be used as a grid variable for cross-section calculations. As described in Section 4.3, a convergence issue was found when coupling SWIFT with other physical models for the full-core GC-MR. It is currently speculated that the issue originates from a numerical conflict between the temperature feedback and hydrogen feedback. Further investigations will be needed to address such an issue.

Two computational resources were used for the MultiApp-based simulations discussed in this report. The small-scale and testing simulations were run on Argonne's divisional cluster, where the separate MOOSE applications were compiled separately using a shared MOOSE build and were dynamically linked with each other during execution. In contrast, the large-scale simulations were run on INL's HPC. On INL-HPC, simulations that did not involve SWIFT were run using the precompiled BlueCRAB executable, whereas the SWIFT-related simulations were run using a user-built BlueCRAB dynamically linked with a user-built SWIFT (since it is not deployed as part of BlueCRAB).

With the development of this project, the modeled scale has expanded from one unit cell in FY-2021 [3], through one assembly, to the current full core models for all the investigated microreactor types. Such an expansion in model scale has also led to higher demand for computational resources (partly compensated by improved code performance throughout the years). In FY-2024, it was found that a distributed mesh approach along with mesh pre-splitting is essential to run these full core multiphysics models without using impractical amounts of resources. This approach is mainly

to save memory consumption on each HPC node. During the complete transition from replicated meshes to distributed meshes, some Transfer approaches that were only applicable to replicated mesh were replaced by alternative approaches that are fully compatible with distributed mesh.

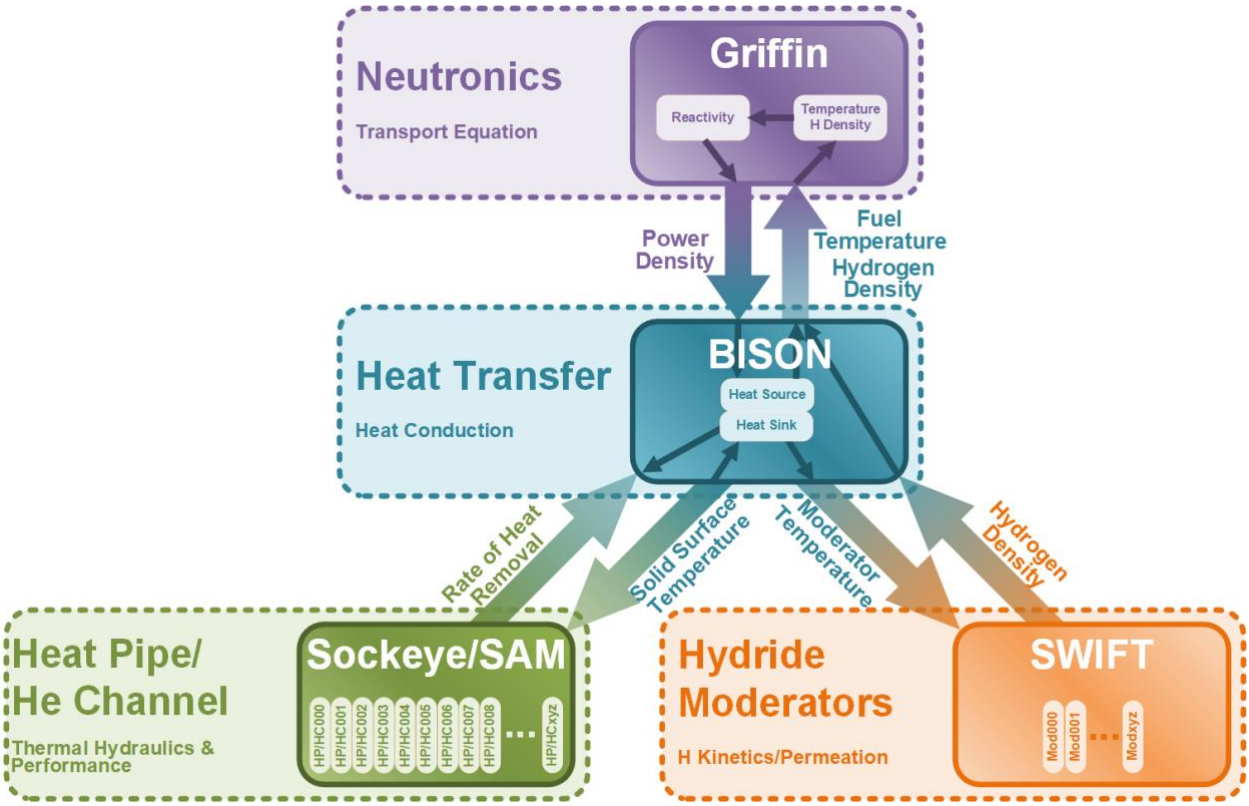

Figure 2-1. MultiApp hierarchy for the multiphysics simulations considered in this report.

3 Analysis of a Full-Core Heat Pipe MicroReactor (HP-MR)

The HP-MR was designed at ANL in FY-2021 as a modeling experiment gathering non-conventional technologies employed in the microreactor industry that may challenge modeling and simulation tools. The HP-MR is a 2MW thermal reactor shown in Figure 3-1 using TRISO fuel with 19.95 at% Low-Enriched Uranium (LEU) in a hexagonal graphite matrix [3]. 30 fuel assemblies are surrounded by one ring of beryllium reflector and 12 control drums. This concept employs heat pipes with stainless-steel envelope and potassium as the working fluid, and Yttrium-hydride (YH_2) moderator pins.

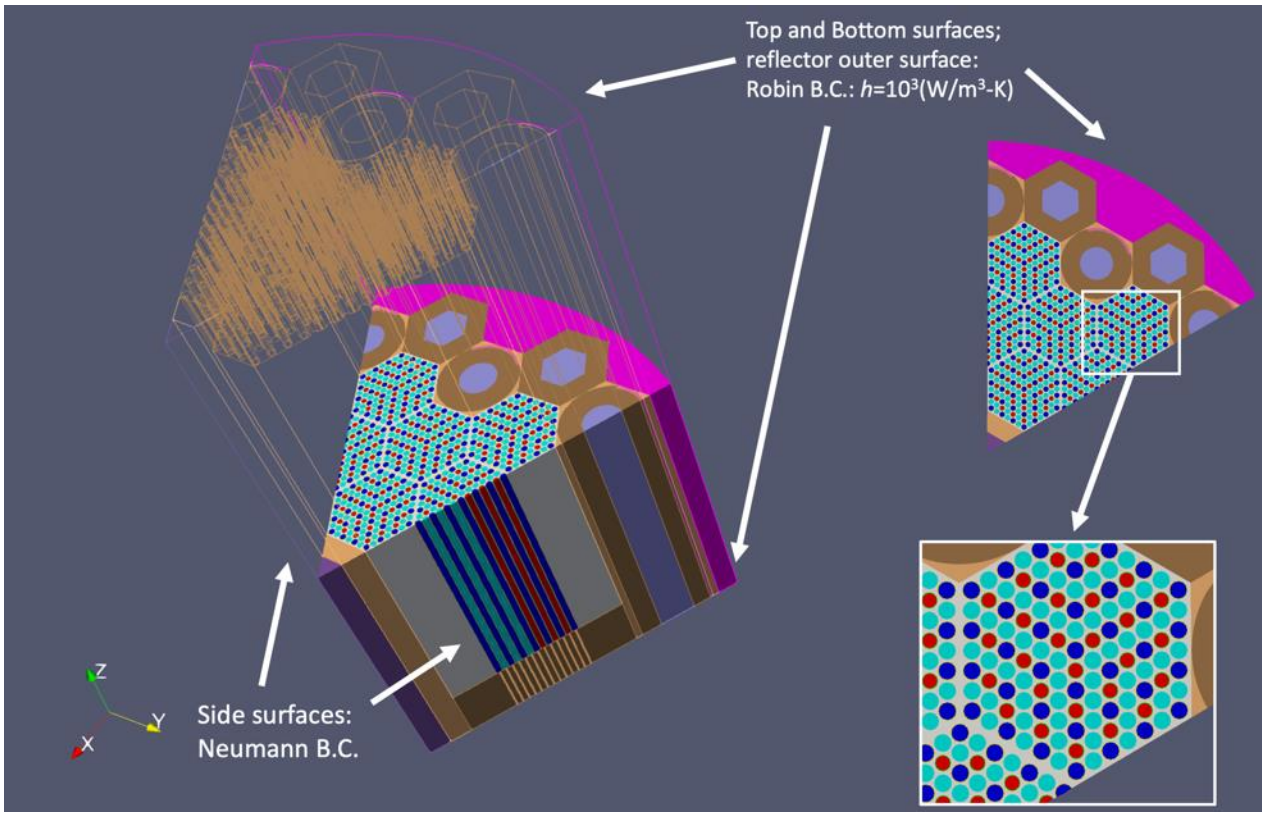

Figure 3-1. Description of the HP-MR full-core model.

Previous work [3] [4] [5] focused on unit cell and full-core analysis, where multiphysics steady-state and multiple transients models were developed. Work on the HP-MR models continued in FY-2024 with 3 separate activities:

- The multiphysics transient models developed in FY-2023, involving Griffin (neutronics), BISON (heat conduction) and Sockeye (heat pipe modeling) were improved in FY-2023 by including SWIFT for H_2 redistribution analyses in hydrogen leakage transient in Section 3.2. This required additional neutronic verification benchmark analyses on cross-section interpolation approach, as performed in Section 3.1. Demonstration of modeling of inadvertent control drum rotation is proposed in Section 3.4.
- Sockeye's "vapor-only" solver was tested and demonstrated through the development of a startup transient based on the unit cell multiphysics model described in [3], as discussed in Section 3.3.

- BISON capability to model TRISO failure probability initiated in FY-2023 was improved by incorporating the latest mechanical models for monolithic silicon carbide layer. The implications of the improvements and the steady-state performance of TRISO particles are summarized in Section 3.5.

3.1 Updated neutronic model

Neutronics calculations are performed with Griffin DFEM-SN with CMFD solver. The multigroup cross sections used in this study were derived from the Monte Carlo Serpent-2 code. Only one set of cross sections for all fuel rods was generated by averaging among all fuel regions in the Serpent model (i.e., the same multigroup cross sections are considered in all axial fuel regions of every assembly). Various sets of temperature-dependent cross sections and different energy group numbers were generated. Another grid dimension of the tabulated cross sections accounts for variations in hydrogen content in the hydride moderator, which is required for multiphysics simulations involving SWIFT analyses. It should be noted that the He-gap is explicitly modeled both in Serpent-2 for generating the multigroup cross sections and in the transport Griffin model of the core.

Verification of our multidimensional cross-section interpolation methodology was conducted in FY-2021 as outlined in Ref. [18], and was reproduced this FY based on the latest reference HP-MR full core model as fully reported in [19]. The effective multiplication factor (keff) shown in Table 3-1 was obtained from the Griffin DFEM-SN method using three polar angles and six azimuthal angles in SN, and the maximum scattering anisotropy is 2, with CMFD employed for acceleration. Eigenvalues were estimated at three different temperature points and compared against reference Monte Carlo Serpent-2 results.

Table 3-1. keff and net temperature reactivity feedback estimates from Griffin at various temperature points, compared to Serpent-2.

	700 K	**800 K**	**1000 K**
Serpent-2 keff [a] Doppler [b] *(pcm/K)*	 1.03143 Ref.	 1.02853 -2.73	 1.02286 -2.69
Griffin keff [a] Doppler [b] *(pcm/K)*	 1.03456 Ref.	 1.03204 -2.36	 1.02572 -2.98
Δ keff *(pcm)* Δ Doppler	-313 n/a [c]	-351 -14%	-286 +11%

[a] ±7.5 pcm.
[b] Calculated from 700 K, ±0.03 to 0.1 pcm/K.
[c] n/a = Not applicable

Temperatures were the same in the fuel, moderator, and structure regions and changed simultaneously while the reactor geometry remained the same. The Doppler coefficients (for fuel, moderator, and structure regions) were estimated between 700 K and 800 K, and between 800 K and 1000 K, as shown in Table 3-1. In the interval between 700 K and 800 K, the Doppler reactivity was estimated to be −2.73 pcm/K with Serpent-2 and −2.36 pcm/K with Griffin, showing a

discrepancy of about −14%. An 11% discrepancy was noticed for the interval from 800 K to 1000 K.

Similar analysis is summarized in Table 3-2 with different H content points. First, the reduction in H content is observed to lead to a strong reduction in keff. It should be noted that the error in the keff estimate increases at lower H content (up to 514 pcm at x = 1 from 313 pcm at x = 2). Even though potentially concerning and worthy of further investigation, this discrepancy has a relatively small effect on the accuracy of the Multiphysics simulations due to the relatively good estimate of the H coefficient using Griffin, with less than 6% of discrepancy (slightly underestimated) when compared with Serpent-2. Improving agreement at different temperature and hydrogen content points may be achievable through further refinement of the homogenized multigroup cross sections and mesh. It should be noted that the cross-section library contained a grid specifically tailored to various hydrogen contents, including x = 1, x = 1.5, and x = 2.0, where no interpolation was necessary. The H coefficient in Table 3-2 represents the net reactivity change due to variations in hydrogen content compared to the reference hydrogen content considered for nominal conditions.

Table 3-2. keff and Hydrogen content coefficient from Griffin
at various H-content points in YHx, compared to Serpent-2, at T=700K.

		YH_1	**$YH_{1.5}$**	**YH_2**
Serpent-2	keff [a]	0.96970	1.01243	1.03143
	H coef. [b] *(pcm)*	-4352	-1819	Ref.
Griffin	keff [a]	0.97484	1.01657	1.03456
	H coef. [b] *(pcm)*	-4211	-1711	Ref.
Diff	Δkeff *(pcm)*	-514	-414	-313
	ΔH. coef.	3%	6%	n/a

[a] ± 7.5 pcm

[b] Calculated from YH_2, ± 11 pcm

In Table 3-2, the reference moderator composition is YH_2. This analysis complements the findings in [18], confirming that the cross-section interpolation approach utilized in Griffin sufficiently accommodates variations in temperature and hydrogen content.

Figure 3-2 illustrates the axial power distribution, plotted at the central height of each axial node, using DFEM-SN (3,6) with CMFD at 700 K, demonstrating good agreement with the reference Serpent-2 results at the same temperature. A small discrepancy in power distribution at the interface with the axial reflector might come from the spectrum difference at the end of the fuel pin with neutrons returning back from the reflectors. The generated multigroup cross section in this region of the core may help further reduce these power discrepancies.

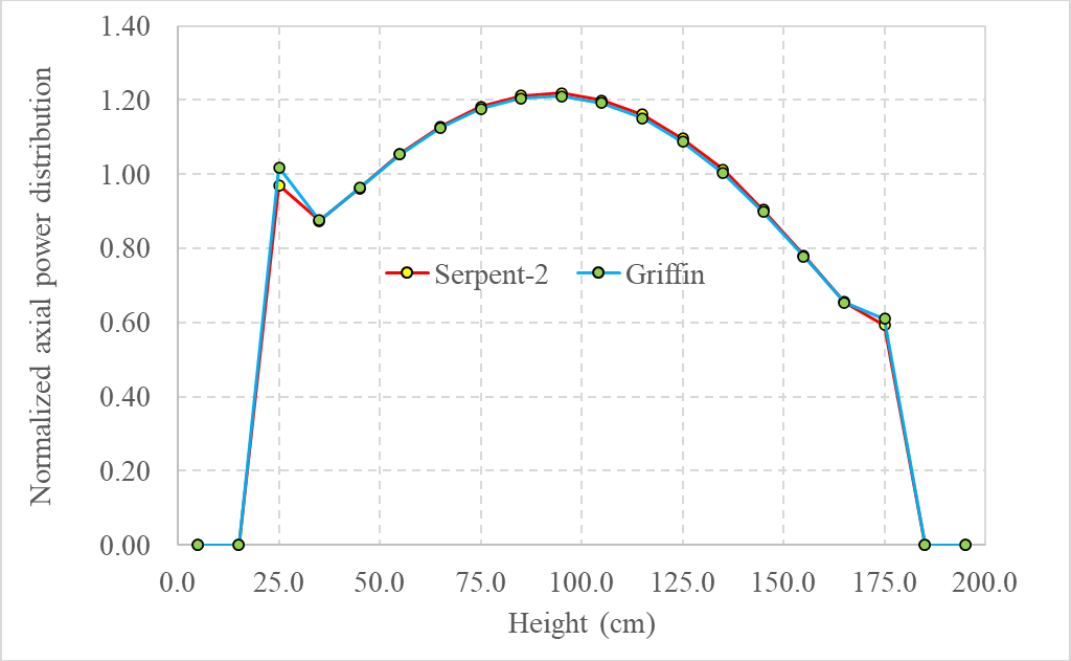

Figure 3-2. Comparison of the axial power distributions calculated by Griffin and Serpent-2

3.2 Hydrogen leakage transients

Compactness is a key target for microreactors vendors. To achieve this, moderation solutions that surpass conventional graphite moderators are employed by some vendors. Metal hydrides, particularly yttrium hydride and zirconium hydride, have been considered for use as inserted enhancement moderation modules within a microreactor's graphite matrix. However, metal hydrides are subject to thermal dissociation at elevated temperatures. Therefore, a hydrogen-impermeable enclosure is typically used to clad the hydride pellet, maintaining a sustainable hydrogen partial pressure. Even with the enclosure, hydrogen can still slowly permeate and escape, leading to a loss of moderation capability. Additionally, driven by chemical potential, hydrogen tends to migrate towards the cooler part of the hydride. In the presence of a temperature gradient, a hydride moderator is subject to hydrogen redistribution, which also affects neutronics. To capture these phenomena, SWIFT needs to be coupled with other microreactor physics models for both steady state and transient simulations.

3.2.1 *Implementation of SWIFT into full-core HP-MR model*

To implement the SWIFT hydride performance model into the full core HP-MR simulation, the $YH_{1.94}$ moderator with uniform hydrogen distribution was used as an initial condition in the SWIFT simulation. Since initial steady-state simulation is required to initiate the multiphysics simulation, the permeation of the moderator cladding was artificially disabled to ensure that the multiphysics steady-state simulation could achieve convergence. The main focus of the SWIFT simulation is the redistribution of hydrogen within the moderator under the temperature gradient during normal operation. For follow-up transient simulations, the permeation of the moderator enclosure system can be activated at the beginning of the transient simulation to evaluate its impact on HP-MR performance.

3.2.2 *Steady-state performance*

To predict reactor performance during steady-state operation, a Dirichlet temperature boundary condition of 800 K was utilized on the condenser side of the heat pipe. The coupling scheme shown in Figure 2-1 was applied, with two simulations completed: one accounting for hydrogen redistribution and one without. Results for both approaches are summarized in Table 3-3. This steady-state simulation took approximately 43 hours and 8 hours, respectively, for the model set with and without SWIFT inclusion, using 240 Message Passing Interface ranks on 10 nodes of 48-core CPUs. For the steady-state simulation with SWIFT, it took 260 Richardson iterations in the main (Griffin) application and 15 iterations in the BISON application to converge (compared to 31 Richardson iterations in Griffin and 15 iterations in BISON for the non-SWIFT model). It was found that involving SWIFT slows convergence because the neutronics calculation is highly sensitive to changes in hydrogen content.

As expected from heat pipe reactor systems, the temperature variations across the core are minimal, with fuel and moderator temperatures varying from 814 K to 866 K. The temperature profiles are also shown in Figure 3-3 and average/peak temperatures are summarized in Table 3-3. Because of the uniform temperature distribution across the core, the keff estimated by the isothermal Griffin simulation (core at 800 K) is relatively close to the steady-state solution: 60 and 105 pcm from the steady-state solution with and without SWIFT, respectively.

Despite the relatively small temperature gradients, the hydrogen content within the YH_x moderator estimated with SWIFT is found to vary from 1.90 to 2.0 (see Figure 3-3). Lower hydrogen content is found in the warmer part of the core, toward its center. Although the impact on core temperatures is limited when accounting for hydrogen migration, it is more significant on the eigenvalue estimate (45 pcm), where neglecting the hydrogen redistribution leads to overestimating keff by predicting higher hydrogen content toward the center of the core.

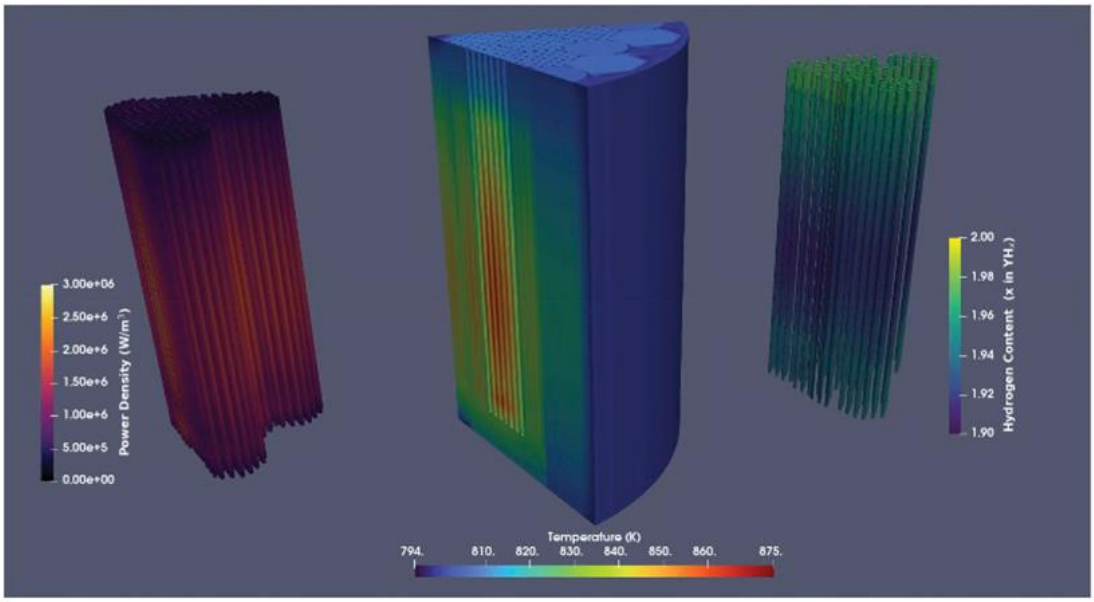

Figure 3-3. Key simulation results of steady-state HP-MR operating at nominal power.

Table 3-3. Comparison of some key predicted parameters by HP-MR models with and without SWIFT implementation.

Parameter	**w/ SWIFT**	**w/o SWIFT**
Power (kW_{th})	345.6	345.6
$T_{fuel,\ avg}$ (K)	843.50	843.51
$T_{fuel,\ max}$ (K)	866.05	866.28
$T_{fuel,\ min}$ (K)	814.31	814.27
$T_{mod,\ avg}$ (K)	842.16	842.17
$T_{mod,\ max}$ (K)	861.99	862.67
$T_{mod,\ min}$ (K)	814.72	814.67
keff	1.03269	1.03317

3.2.3 *Demonstrative hydrogen leaking transient*

While more intense investigations on the hydride model and its impacts on microreactor performance were made for the GC-MR model, which will be covered in a Section 4.3 of this report, some brief demonstrative efforts were also made to explore the impact of hydrogen leakage for the HP-MR full-core models. Specifically, an artificial welding failure incident applied to all the moderator envelopes of the HP-MR core was introduced at the beginning of the transient simulation. The permeability of the welding parts of all the hydride moderator modules was artificially assigned a large value (0.0001 $mol_{H2}/m/s/Pa^{1/2}$) to initiate fast hydrogen leakage.

Keeping all other conditions unchanged, the transient simulation was run for 10,000 seconds to observe the response of the HP-MR to such changes in the hydride moderator. As shown in Figure 3-4(a), the maximum YH_x decreased from the original 1.9758 to 1.9752, which is minor but non-negligible. As a result, the loss of hydrogen slightly reduced the reactivity and eventually led to a ~0.1% power drop and consequently less than a 0.05 K fuel temperature change (Figure 3-4(b) and (c)). Therefore, it is evident that even an exaggerated hydrogen leakage event causes very minor changes in microreactor performance over a couple of hours, which is a considerable length of time for any conventional transient scenarios. That is, although hydrogen leakage would lead to long-term reactivity issues, it barely has any significant short-term effect. Therefore, this analysis demonstrates it might be acceptable to omit the evolution in the hydride moderator when simulating conventional transient scenarios in HP-MR.

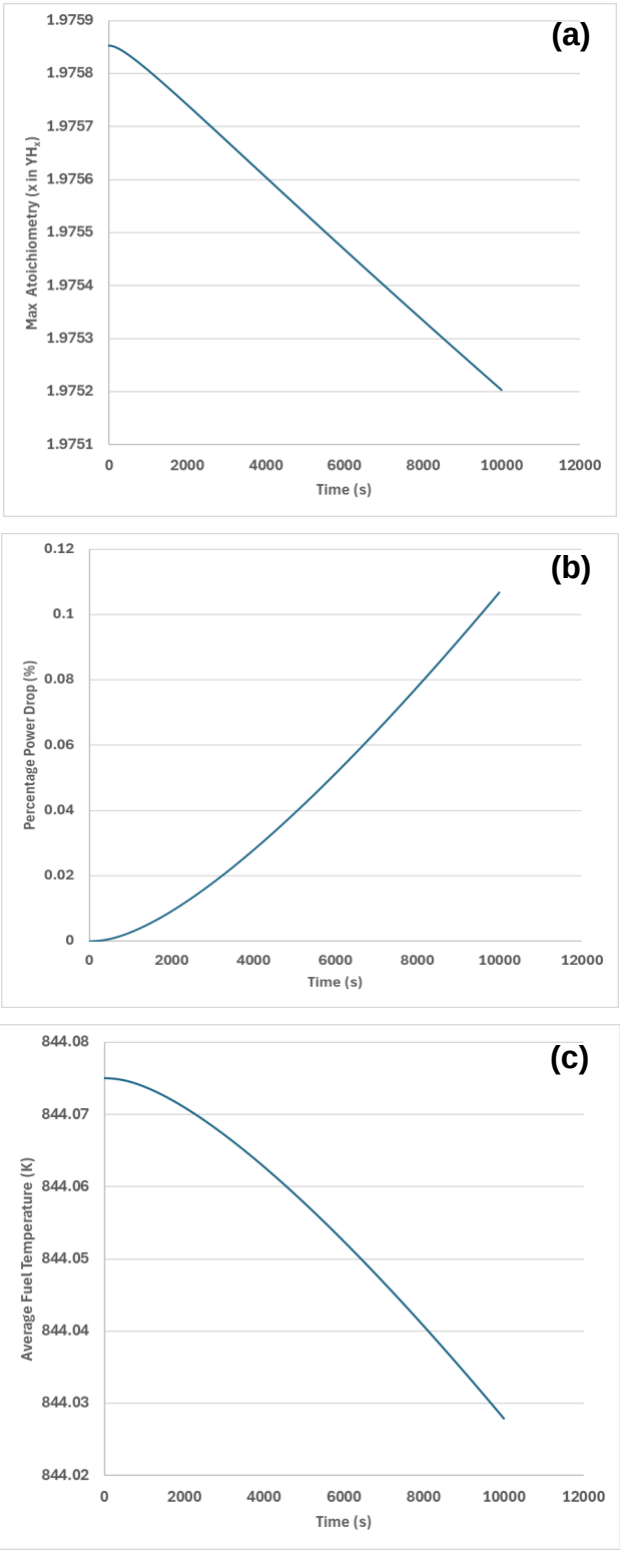

Figure 3-4. Time evolution of maximum hydride stoichiometry, percentage power drop, and average fuel temperature during the simulated HP-MR hydride leaking transient.

3.3 Startup transients analysis (vapor-only flow model)

Reactor startup transient models temperature increase from cold to hot condition and from zero power to 100% power. This power increase results in a phase change within the heat pipe. The working fluid transitions from solid to liquid to vapor. This becomes especially challenging to model, which is why typical heat pipe solvers use approximation.

The vapor-only model developed in Sockeye generalizes the formulation. This model has been assessed with startup transient conditions and a user tutorial for training of industry partners has been completed. This tutorial is in the submission process to become part of the Sockeye user documentation [17]. The unit-cell test case with the vapor-only model is in the process of being extended to full-core multiphysics simulations under startup transient conditions.

A single heat pipe is subjected to an input power generated by the fuel in a unit cell model that was described as a multiphysics tutorial for Sockeye in FY-2023 [5]. The input power at the evaporator region follows the time series shown in Figure 3-5.

For this MOOSE/Sockeye demonstration, the mesh for the unit cell is provided, and is consistent with the Startup transients analysis with the Vapor-Only Flow Model modeled in FY-2023 [5]. The mesh contains the fuel, moderator, graphite matrix, and reflectors components. The location at the center of the unit cell is for the heat pipe modeled with Sockeye. The temperature distribution from the modeled unit cell with the heat pipe is shown in Figure 3-6. The schematic and specifications of the heat pipe modeled are consistent with the unit cell model that was developed as a multiphysics tutorial for Sockeye in FY-2023 [5]. Effort in FY-2024 focused on improvements to documentation in resolving comments brought up during review process.

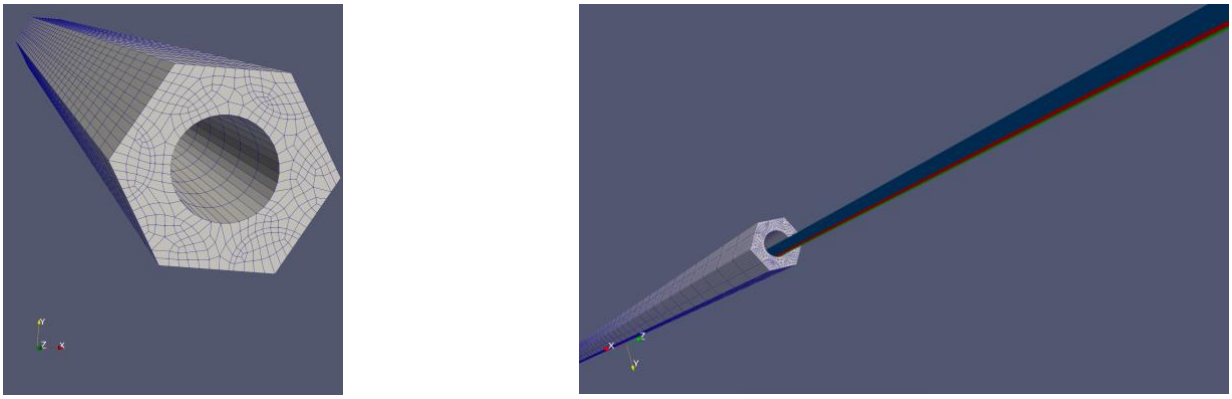

Figure 3-5. Mesh of unit cell assembly. Left: Without heat pipe; Right: With heat pipe.

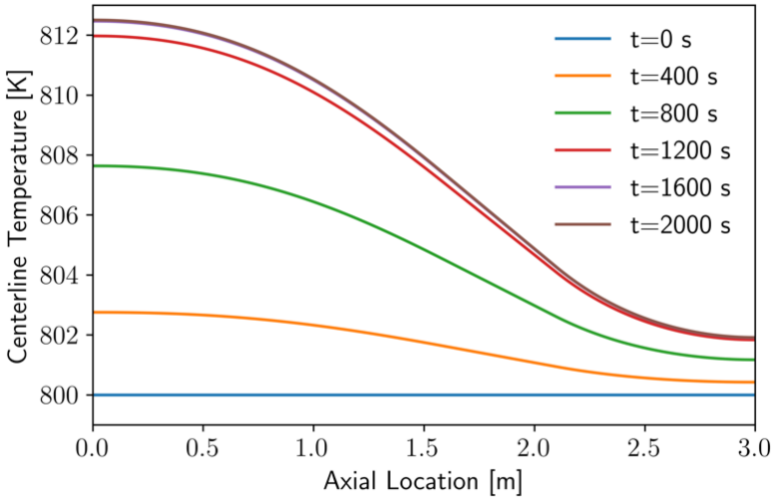

Figure 3-6. Centerline (vapor core) temperature profile at multiple time steps.

This demonstration start-up model has been expanded to perform a start-up multiphysics analysis of the full core heat pipe microreactor (HP-MR). The goal of this demonstration is to develop a high-fidelity model of the full-core HP-MR of a reactor start-up transient to be published on the VTB as a demonstration of the multiphysics capabilities for heat pipe modeling.

Sockeye can be coupled to other MOOSE-based applications. The primary mode of coupling is through heat transfer boundary conditions between the applications, specified from either heat flux or temperatures of each side of the heat pipe to allow multiphysics simulations. In the HP-MR pipe model, "multiphysics" refers to the two-dimensional (2-D) heat conduction model of the domain including the heat pipe cladding and core block, coupled to the Sockeye heat pipe model. The domains are treated separately and coupled via a convection interface condition. This work uses the newest vapor-only model in Sockeye to mimic the working fluid operational (steady-state and transient) conditions and startup/shutdown heat pipe performance Startup/shutdown conditions are simulated with the heat pipe starting at the cold temperature and heat flux boundary conditions. Below the melting temperature of the fluid, properties of the solid phase are approximated to be equal to the liquid properties evaluated at the triple point of the fluid, and the latent heat of fusion is neglected when crossing the melting point.

The heat pipe is divided into three radial regions: (1) the cladding, (2) the wick/annulus, and (3) the vapor core. It is assumed that the liquid and vapor masses and volumes are fixed in their respective radial positions. The wick region uses a weighted average of liquid and wick material properties. This work is currently undergoing development and it is expected to be completed and uploaded on the VTB as part of the high fidelity multiphysics modeling database in early FY-2025.

3.4 Control drum rotation simulation

Inadvertent reactivity insertion accidents are required transients scenarios considered by industry for NRC licensing. For microreactors, modeling of rotating drums may bring some challenges due to the changes in mesh and to the localized power effects. Those require careful consideration on mesh and cross-section tabulation, together with high-fidelity simulations. Previously, INL documented a HP-MR control drum model [20]. This model was simplified to a 2D geometry,

leveraging symmetry to reduce the domain to 1/12th of the full core. Additionally, heat pipes were simulated using convective boundary conditions rather than using Sockeye to calculate the actual heat removal. In this section, a 3-D Multiphysics control drum rotation model using Griffin, Bison, and Sockeye is introduced. A 1/6 symmetry was used, with the simulation involving the rotation of six drums in symmetric positions.

3.4.1 *Griffin (Neutronics)-only model*

Multi-group cross sections (11 energy groups) were generated using the Monte Carlo Serpent-2 Code, employing three grid structures: control drum rotation angle (4 points), fuel temperature (5 points), and temperatures for the moderator, reflector, monolith, and heat pipe (4 points). Figure 3-7 illustrates the Serpent-2 model with rotated control drums. As discussed in Section 2.2, the process of creating tabulated cross-sections across multiple grids using the Serpent-Griffin workflow is currently complex. This is because Griffin cannot directly convert the output from Serpent's branching calculations to ISOXML, due to the one-to-one mapping between a file and a grid point (as discussed in Section 2.2). To overcome this challenge, a Python script was developed to automate the generation of the multiple grid ISOXML from Serpent-2.

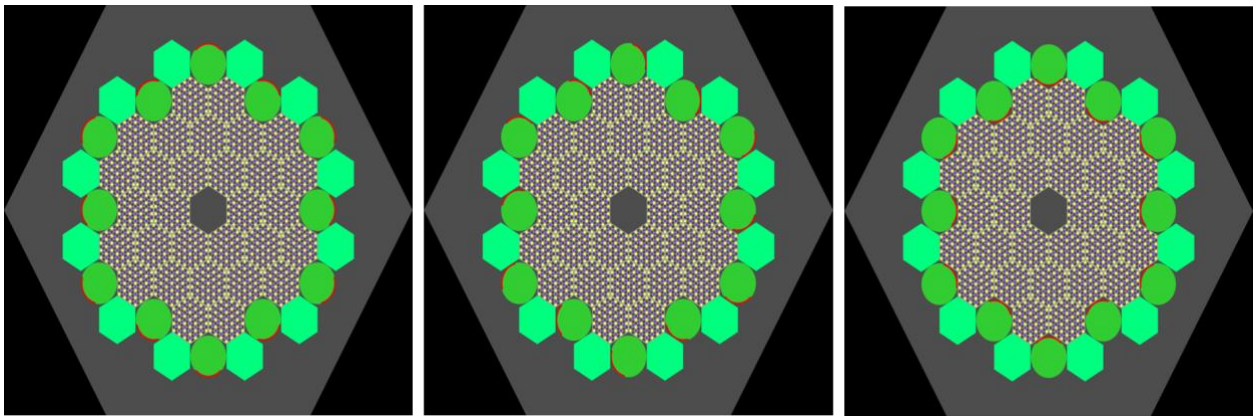

Figure 3-7. Serpent-2 model at various drum rotations used for generating multigroup cross-sections.

For the steady-state stand-alone Griffin simulations, the DFEM-SN solver was used with 3 polar angles and 6 azimuthal angles, along with CMFD acceleration. A comparison was made with the Serpent-2 code for two scenarios: control drums inserted, and control drums withdrawn. Two models were considered for the analysis (as shown in Figure 3-8): Model A, which explicitly models the poison region within the mesh, and Model B, which treats the poison and non-poison regions in the drums as a single block. Model A would be the preferred option to define explicitly the control drum location within the mesh. Model B is a simplified approach used for dynamic control drum rotation modeling, where Griffin input parameters—such as rod_segment_length, front_position_function, rotation_center, and segment_material_ids—are utilized to define the poison and non-poison regions.

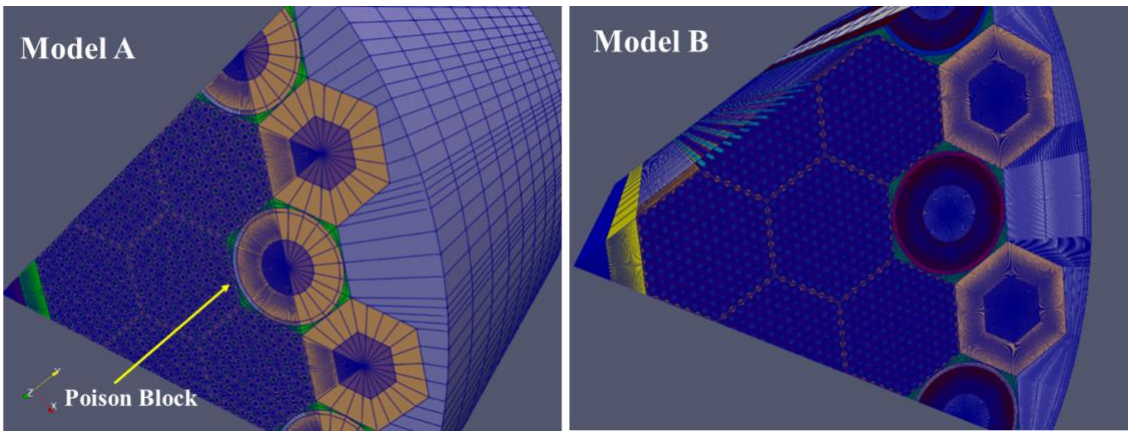

Figure 3-8. Comparison of two different mesh models of 1/6 HPMR for steady-state stand-alone Griffin simulations.

Table 3-4 compares the Griffin and Serpent-2 results for the mentioned scenarios. For Model A with control drums inserted, a discrepancy in K-eff of -422pcm was noted, while for the control drum withdrawn case, discrepancies in K-eff of -356pcm for Model A and 273pcm for Model B were observed. It is also important to note that a significant discrepancy in K-eff of -1,362 was observed with Model B for the control drum inserted case, which requires further investigation.

Table 3-4. Code-to-code comparison between Griffin and Serpent-2 for control drum in and out cases using mesh models A and B.

Case	K_{eff} (Serpent-2)	Model	K_{eff} (Griffin)	Δ Keff [pcm]
Drums out	1.04130 ±00007	A	1.044869	-356
Drums out		B	1.038570	273
Drums in	0.935949 ±00009	A	0.940171	-422
Drums in		B	0.949575	-1,362

As discussed in Section 2.2, the treatment of the cusping effect in Griffin is still under development. To address this, the mesh needed to be refined so that the drum's front aligned with the element edges at each time step, as illustrated in Figure 3-9.

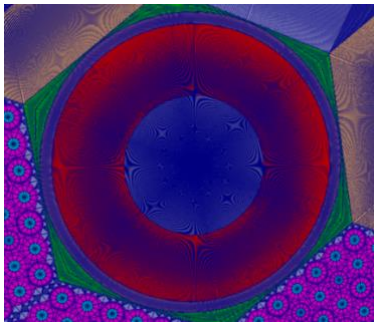

Figure 3-9. Mesh refinement in the control drum regions.

For the standalone neutronic model of the control drum rotation, a 3-D whole core with 1/6 symmetry was used. Reflective boundary conditions were applied along the symmetry lines, while vacuum boundary conditions were used on the top, bottom, and side boundaries. The drum indicated in Figure 3-10 was subject to rotating movement during the simulation. Initially, it was inserted by 40 degrees to achieve core criticality. Given the 1/6 symmetry, the rotation or insertion this drum represents the rotation of six drums in the core.

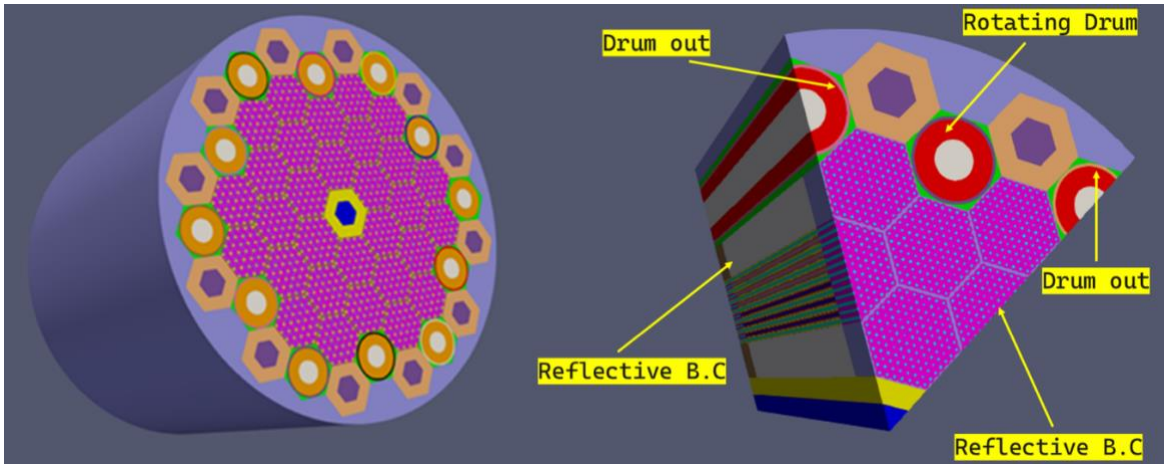

Figure 3-10. Whole core HPMR (left) and 1/6 HPMR with reflective boundary condition used in the Griffin transient simulation, showing the rotating drum.

Two scenarios were analyzed. In scenario I, the drums accidentally rotate outward by 5 degrees per second for 1 second, then inward at the same speed for 2 seconds as the result of an expected corrective action that would reinsert the control drums. In Scenario II, drums accidentally rotate outward by 20 degrees per second for 1 second, followed by inward rotation at the same speed for 2 seconds. Initially, neutronics-only results are shown in Figure 3-11 and Figure 3-12. In both Figure 3-11 and Figure 3-12, the normalized core power is plotted alongside the control drum rotation. As the control drums rotate outward from their initial position, reactivity is inserted, leading to a power increase shown in Figure 3-11. The rotation speed in Figure 3-12 is much faster (20 degrees per second) compared to Figure 3-11 (5 degrees per second), which explains the significantly larger power spike in Figure 3-12 due to the greater reactivity insertion. After 1 second, the control drums are reinserted at the same speed, resulting in a much faster power decrease in Figure 3-12 due to the higher reactivity insertion rate.

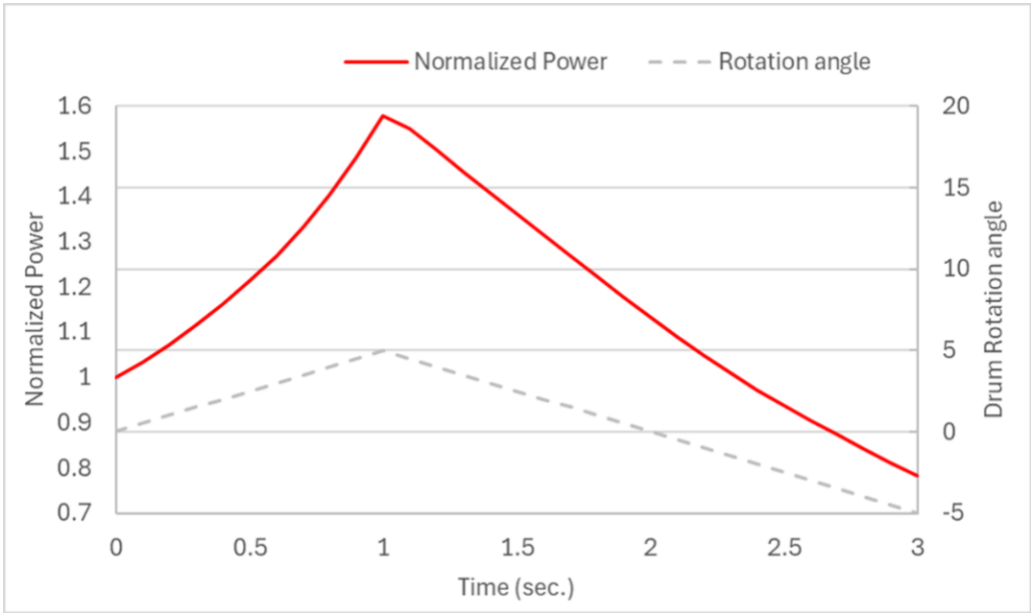

Figure 3-11. Scenario I of inadvertent control drum rotation (Griffin-only).

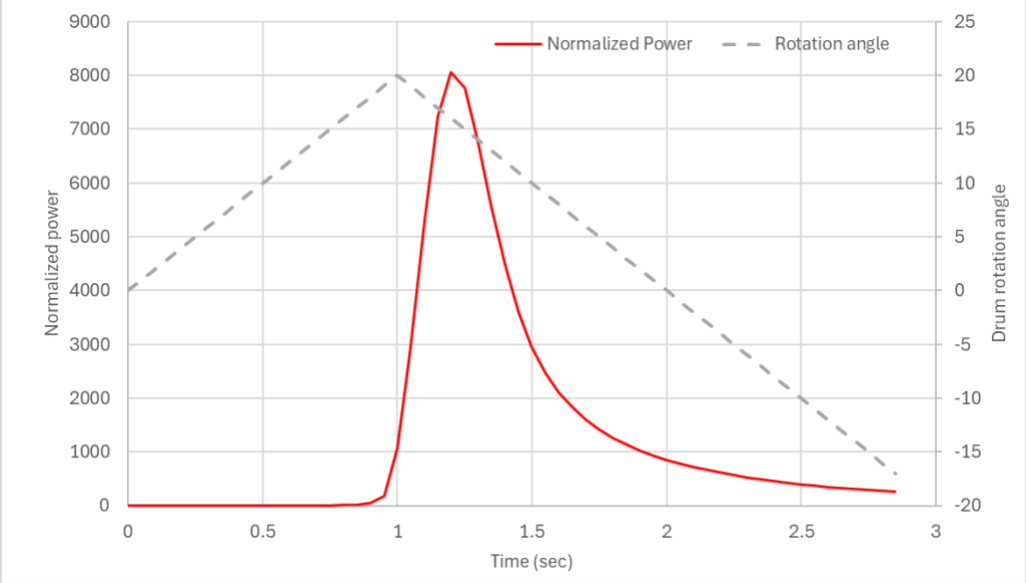

Figure 3-12. Scenario II of inadvertent control drum rotation (Griffin-only).

3.4.2 *Multiphysics model*

The Griffin control drum rotation model was integrated into the HP-MR multiphysic model to simulate the reactivity response of HP-MR to control drum rotation, considering temperature effects. The same three-layer MultiApps hierarchy without SWIFT (to reduce computing cost and justified by the low effect expected from H_2 dissociation on this transient), as previously described, was adopted. Achieving convergence for each time step requires approximately 15 Richardson iterations with the BISON child application and Sockeye grandchild application, making the

multiphysics control drum rotation transient computationally expensive. To reduce the required computational resources, the SN(2,3) NA=2 neutronics-only model was simplified to SN(1,3) NA=2 for multiphysics simulations. Using the multiphysics model, the predicted power increase during control drum rotation is slightly lower than that of the neutronics-only model, primarily due to the temperature effect not captured by the single-physics model (see Figure 3-13). The temperature effect is also illustrated in Figure 3-14. The radial power distribution of the core is shown in Figure 3-15.

As the control drums rotate outward, they introduce positive reactivity, which causes a rapid increase in reactor power. This sudden rise in power results in a prompt change in both fuel and moderator temperatures as they respond to the power ramp-up. The core overall temperature reactivity feedback is negative, meaning it generates negative reactivity to counteract the positive reactivity introduced by the control drums withdrawal. Consequently, a noticeable reduction in peak power occurs during the transient as the temperature feedback takes effect.

After one second of control drum withdrawal, the control drums are re-inserted. This quickly reduces reactor power and temperatures. After three seconds of the transient, both the multiphysics and neutronics-only solutions produced nearly identical power levels. At this point, the moderator and fuel temperatures are below their nominal values, and the control drums are inserted more deeply than they were before the transient.

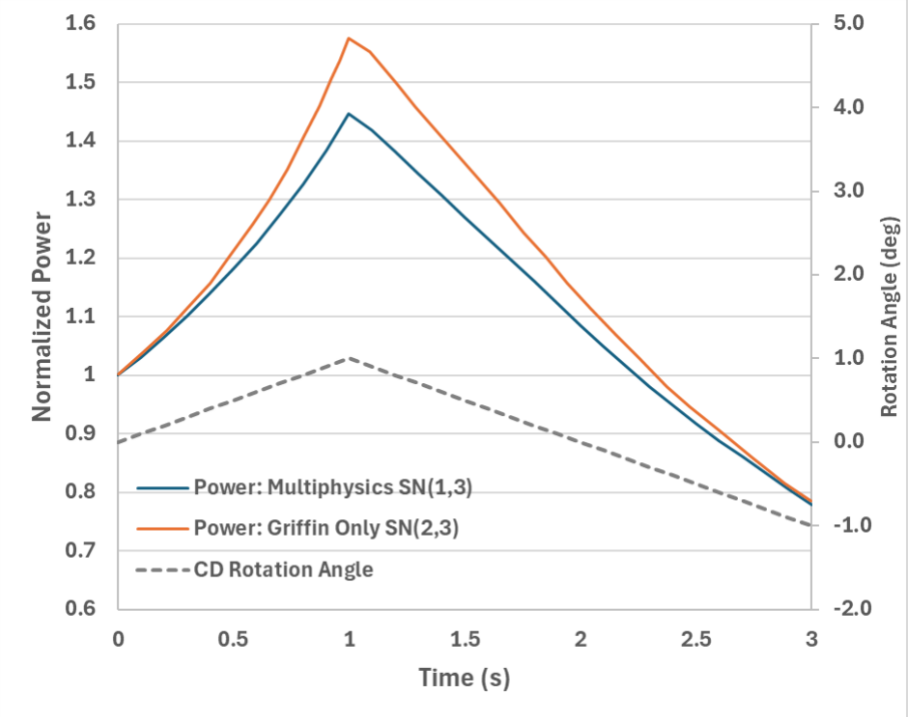

Figure 3-13. Time evolution of HP-MR power due to control drum rotation.

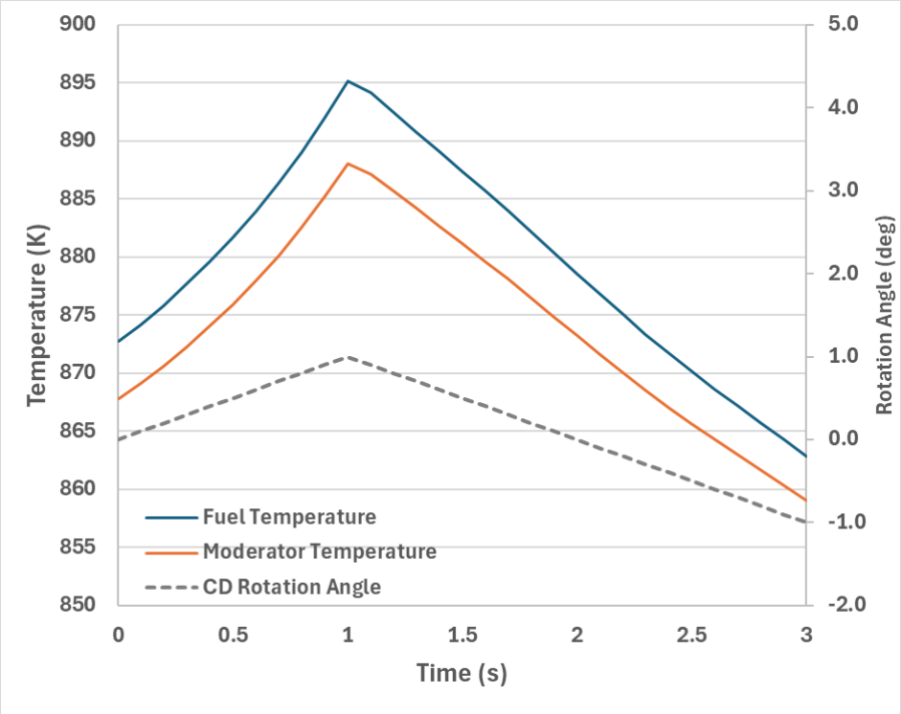

Figure 3-14. Time evolution of the average fuel and moderator temperature due to control drum rotation.

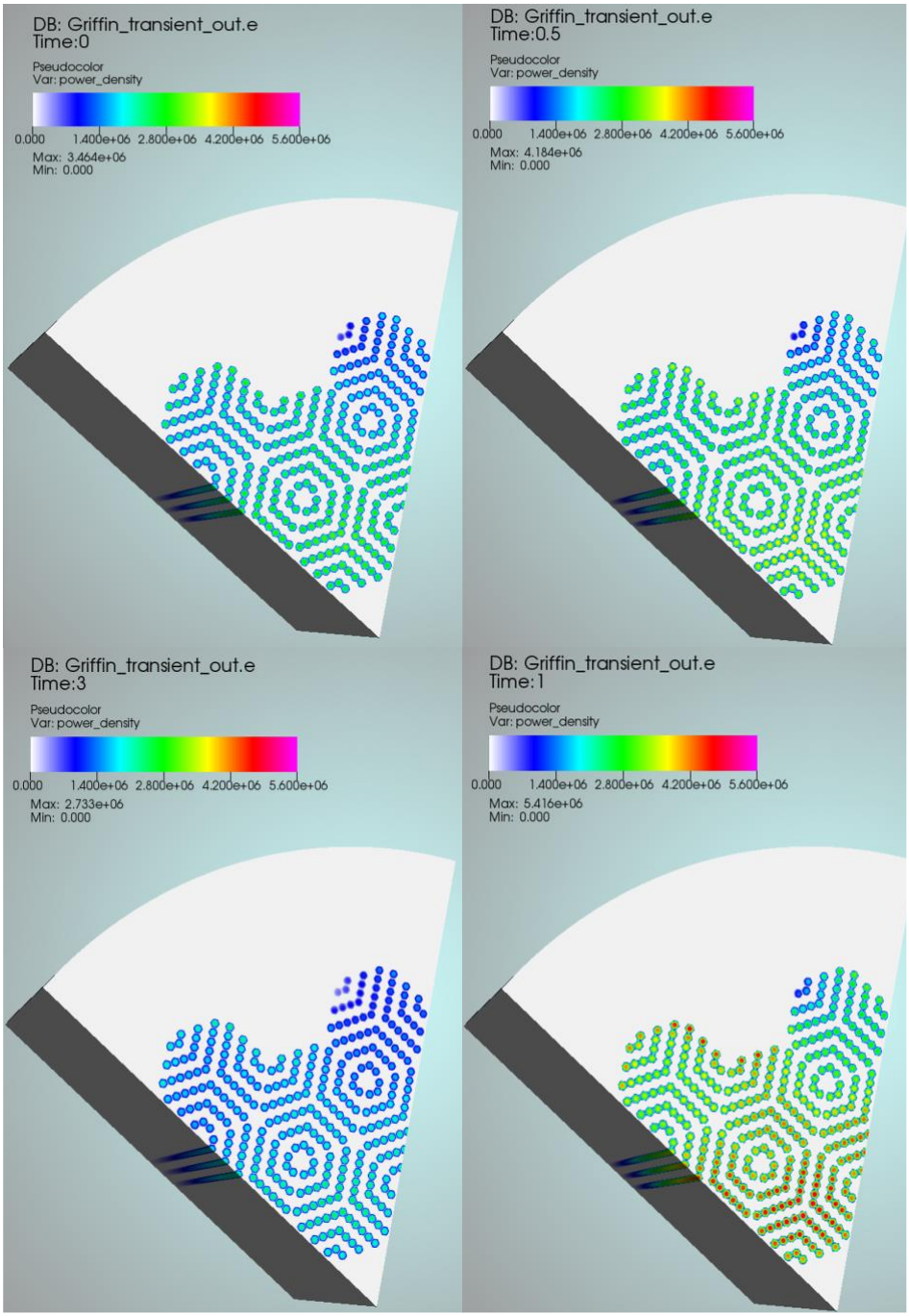

Figure 3-15. Radial view of power at different time steps (neutronic only).

3.5 TRISO fuel performance analysis

The TRISO fuel performance analysis for the HP-MR unit cell multiphysics models developed in FY-2023 [5] has been re-evaluated to incorporate recent enhancements in BISON's TRISO modeling capabilities, as described in Section 2.3. The re-evaluation of TRISO particles in the HP-MR unit cell model was completed, accounting for irradiation-induced deformation effects such as

swelling and creep behaviors in the SiC layer. The TRISO failure probability are modeled on this representative unit-cell throughout 10 years of steady-state irradiation.

Employing the methodology established in FY-2023 [5], one leveraged coupled BISON-Griffin-Sockeye Multiphysics simulations to generate time-varying axial distributions of fuel compact power density, temperature, and hydrostatic stress for a 10-year steady-state fuel cycle. These boundary conditions were integrated into the primary TRISO particle model with the MOOSE Stochastic Tools Module with MultiApp functionality to implement a Monte Carlo sampling method for stochastic analysis. This stochastic analysis was applied to one-dimensional TRISO particles distributed axially along the fuel compact, taking into account microscopic geometrical variations in the TRISO layers among individual particles.

3.5.1 *TRISO fuel performance in the HP-MR*

To identify the implications of the added mechanical models in the SiC layer, the updated TRISO model results were compared to the standard TRISO geometry at one axial location, as shown in Figure 3-16. The introduction of irradiation-induced creep and swelling behaviors in the SiC layer affects the stress distribution within the particle structure. As the SiC layer undergoes creep, it expands, leading to an increase in tensile tangential stress within the inner pyrolytic carbon (IPyC) layer by tensioning the IPyC layer, assuming the bond between the two layers is robust.

Simultaneously, irradiation-induced swelling causes volumetric expansion due to gas and defect formation. As the SiC layer strives to maintain its integrity and resist internal pressure, compressive stress increases as swelling continues. This phenomenon causes the SiC layer to exert pressure against the IPyC layer, reinforcing the compressive stresses within the SiC itself. The updated model demonstrated an increase in Weibull failure probability from 1.3% to 6.1% in the IPyC layer, though no significant change was observed in the SiC layer.

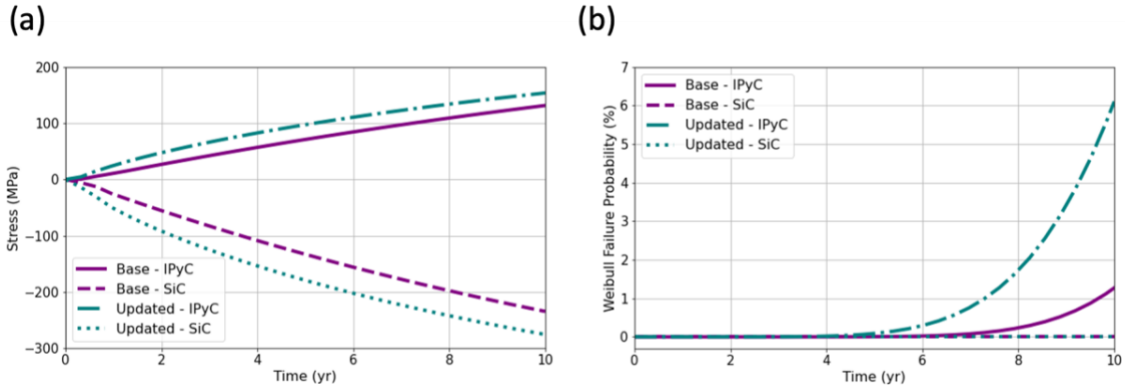

Figure 3-16. Implications of SiC model update one a single TRISO model: (a) tangential stresses and (b) Weibull failure probability.

Given the potential increase in failure probability, stochastic analyses for all axial heights were conducted using the Monte Carlo sampling method. In the master input file, the particle layer widths were provided along with specified standard deviations and bounds. These geometrical variations are sampled using a normal distribution, after which a set of layer coordinates is transferred to the BISON particle simulation input. Upon completion of all simulations, TRISO failure data were extracted using the Transfer system. Prior to the analysis, a convergence study

was performed by increasing the sample size to 50,000, where it was determined that 20,000 samples were sufficient to establish convergence in the results.

Figure 3-17 compares the stochastic analysis results for the base and updated TRISO model during the 10-year steady-state operation. Due to irradiation damage, TRISO particles in the HP-MR unit cell model exhibit increased average IPyC failure rate from 1.1% to 4.1%, while the SiC layer failure rate remains at 0%, representing safe performance of TRISO particles during the steady-state. Although this increase may not appear significant, prolonged irradiation and potential temperature increase during transient scenarios could further elevate the IPyC failure rate, potentially leading to SiC failure due to IPyC cracking.

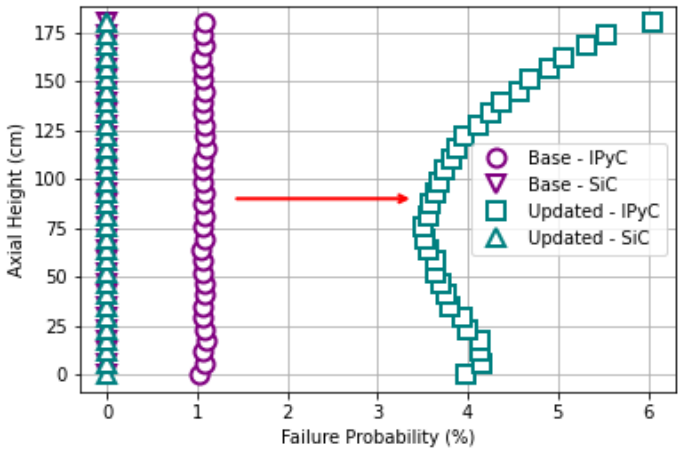

Figure 3-17. Implications of SiC model update: stochastic analysis results.

3.6 Summary of HP-MR work

The work completed in FY-2024 on the HP-MR provided important insight into microreactor behavior enabled through Multiphysics modeling:

- Additional code-to-code verification exercises provided further confirmation of the suitability of Griffin multi-dimensional cross-section tabulation approach (with grids for temperature and hydrogen content). Some of these results were published in a journal paper [19].
- Development of Sockeye startup tutorial was completed for the unit-cell multiphysics model and still needs to be integrated into the Sockeye documentation. Modeling of full-core startup transient was initiated with further work needed in FY-2025. This work will be further extended to apply the new Sockeye mechanistic model in FY-2025.
- Accidental control drum rotations were modeled on the HP-MR, illustrating variations in integrated core power, fuel temperature, and moderator temperature during the accident. The comparison between the neutronics-only and multiphysics solutions demonstrates reasonable physical behavior, emphasizing the impact of temperature feedback on power variations caused by inadvertent control drum movements. While the simulation is

computationally expensive, the coupling of Griffin, BISON, and Sockeye produced reasonably accurate physics behavior through multiphysics integration. Further improvements, such as enhanced cusping treatment in Griffin and reducing memory requirements of the DFEM-SN with the CMFD solver, will improve overall performance and computational efficiency.

- The SWIFT code was coupled with Sockeye, BISON and Griffin for Multiphysics transient simulation of hydrogen leakage transient. This showed relatively slow transient with low impact on core reactivity for the HP-MR, which might be related to the relatively low operating temperature of this HP-MR design and the fast-kinetics transient conditions considered. Analysis on GC-MR in Section 4.3 provides another perspective for very different design with higher temperature gradients. However, this confirms hydrogen modeling can be avoided in case of fast or low-temperature transient.
- Increased probability of IPyC failures when compared to FY-2023, due to the use of improved SiC mechanical models, capturing irradiation induced effects on SiC deformation. However, SiC failure probability is maintained at 0% for the HP-MR. It was recommended to extend this updated model to GC-MR (in section 4.4).

4 Analysis of Gas-Cooled MicroReactor (GC-MR)

Analysis on GC-MR technology was initiated in FY-2022, first focusing on assembly model and industry design [4] then on initial full core [5]. Work on the GC-MR models continued in FY-2024 with several activities:

- The core of the GC-MR was re-designed at the beginning of FY-2024 to enable 1/6 reflective symmetry for reduced computational costs as the initial design proposed in FY-2023 employed rotational symmetry that is not yet supported by Griffin.
- The SWIFT and TRISO failure analyses performed in Section 3 on the HP-MR are also reproduced on the GC-MR that provides different temperature/pressure leading to different behaviors and modeling challenges.

4.1 Detailed GC-MR full-core specifications

The GC-MR model, developed at ANL, serves as a modeling experiment to explore design options considered by microreactor vendors, encompassing features like control drums, hydride metal, and TRISO fuel. This horizontal gas-cooled microreactor system displays a thermal power of 20 MW and an approximate lifespan of 9.5 years. Its power conversion cycle utilizes a Brayton cycle, circulating high-temperature (650°C-850°C) and high-pressure (7 MPa) helium coolant. Surrounding the core are BeO radial and axial neutron reflectors, with twelve control drums positioned in the reflector encircling the core. Control rods, containing 96%-enriched B_4C, are inserted into holes within the middle core assemblies. Displayed in Figure 4-1 and Figure 4-2 are radial and axial views of the core.

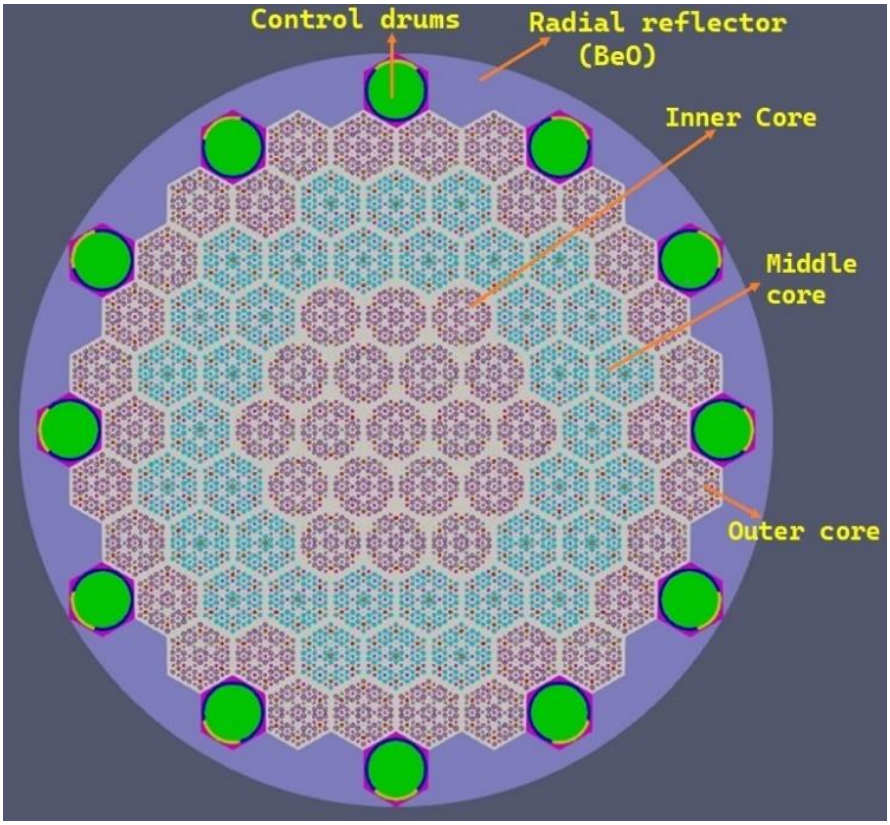

Figure 4-1. Radial view of the GCMR core.

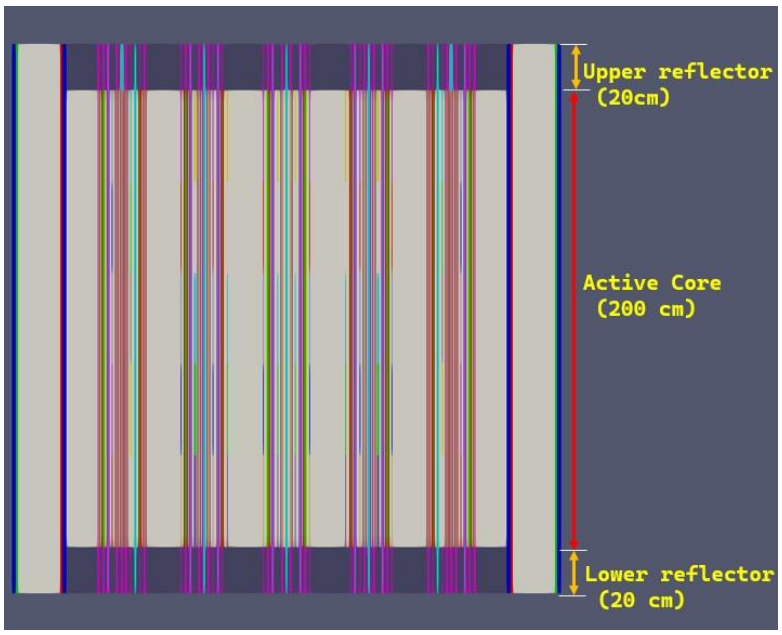

Figure 4-2. Axial view of the GCMR core.

The core comprises three types of fuel assemblies: Assembly A in the inner region, Assembly B in the middle, and Assembly C in the outer core region. Each fuel assembly incorporates TRISO fuel blocks containing 19.75 wt% of LEU fuel and Yttrium hydride moderator pins encased in FeCrAl envelopes. Additionally, burnable poison blocks, composed of Gd_2O_3 particles with a 25% packing fraction distributed axially, and Helium coolant channels. Assembly A's detailed design is provided in Figure 4-3**,** while Figure 4-4 illustrates the design differences among the three assemblies. Assemblies B and C are nearly identical, except for the presence of a central shutdown rod location in assembly B. Each of assemblies B and C is equipped with 6 burnable poison rods, 6 moderator pins, and 48 fuel rods. In contrast, Assembly A contains 12 burnable poison rods and 42 fuel rods. The key design parameters of the GC-MR are summarized in Table 4-1.

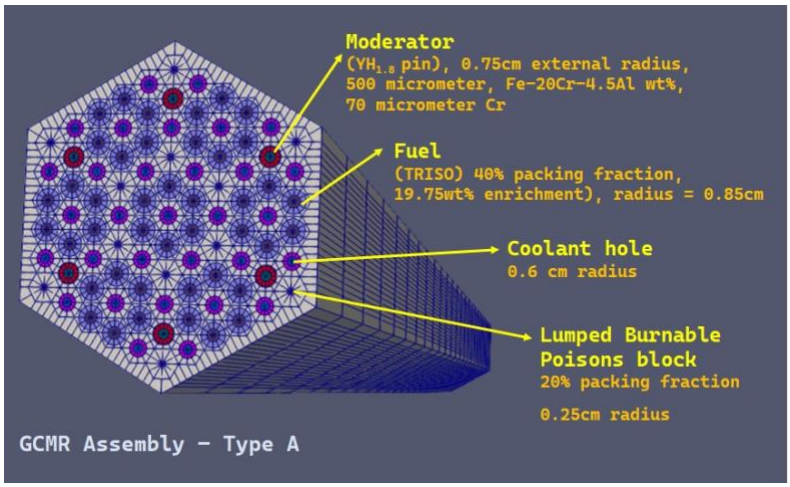

Figure 4-3. GCMR assembly of Type A.

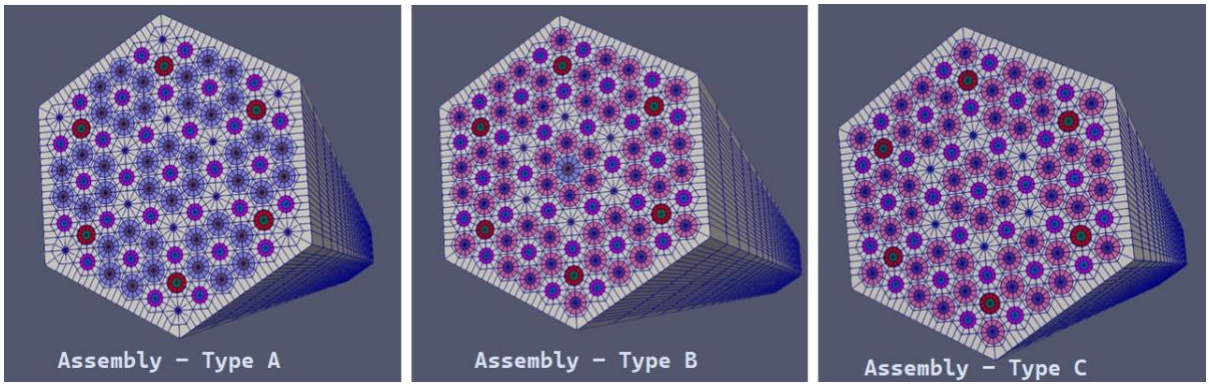

Figure 4-4. Design of the three types of fuel assemblies in the core.

Table 4-1. Main design parameters and dimensions for the GC-MR.

Parameter (unit)	**Value**
Reactor Power (MWth)	20.0
Core diameter (cm)	242.0
Core height (cm)	240.0
Active height (cm)	200.0
Different radial core zones	3
Number of control drums	12
Lattice pitch (cm)	20.8
Pin pitch (cm)	2.0
TRISO fuel compact radius (cm)	0.85
Moderator compact radius (cm)	0.75
Cr coating thickness (cm)	0.007
FeCrAl envelope thickness (cm)	0.05
Burnable poison compact radius (cm)	0.25
Coolant compact radius (cm)	0.6
Control compact radius (cm)	0.95
Fuel	TRISO, 40% packing fraction
Coolant	He
Moderator (Coating, Envelope)	YH1.8 (Cr, FeCrAl)
Burnable poison absorber	Gd2O3 particles, 25% packing fraction
Control rod	B4C (96% B-10 enrichment)

4.2 GC-MR mesh description and neutronic verification

MOOSE's Reactor Module was used to create the mesh structure for the entire core of the GC-MR reactor. Figure 4-5 illustrates a depiction of the 3-D GCMR, detailing both the axial and radial discretization.

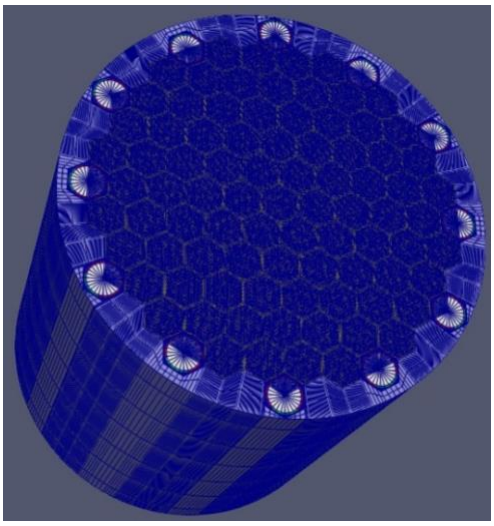

Figure 4-5. Detailed 3-D GCMR core mesh.

Efforts were dedicated to simplifying the 3D whole-core GC-MR mesh to alleviate computational demands, with careful consideration to avoid excessive mesh sizes, particularly in specific regions like the radial reflector and control drum areas, to ensure proper convergence of Griffin. Segmentations of the whole-core GC-MR mesh utilized in the analyses, employing DFEM-SN with CMFD and an 11-energy-group structure, are illustrated in Figure 4-6. The simulation was conducted for 1/6 of the core with reflected boundary conditions on the cut surfaces and vacuum boundaries for the remaining surfaces. The resulting k-eff value for 2 polar angles and 3 azimuthal angles in the SN was determined as 1.051468, reasonably aligning with the k-eff value obtained from the Monte Carlo Serpent-2 code, which is 1.054670 ± 16 pcm. It was determined that an even closer alignment could be achieved with higher numbers of polar and azimuthal angles. Figure 4-7 displays a comparison between the normalized axial power distribution computed by both Serpent-2 and Griffin for DFEM-SN (n_polar=2,n_azimuthal=3) with CMFD, demonstrating good agreement between both tools for the GC-MR neutronic modeling.

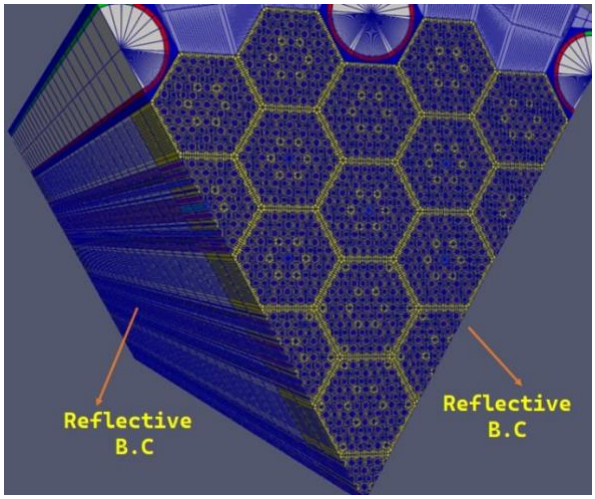

Figure 4-6. 1/6 GCMR core with reflective boundary condition.

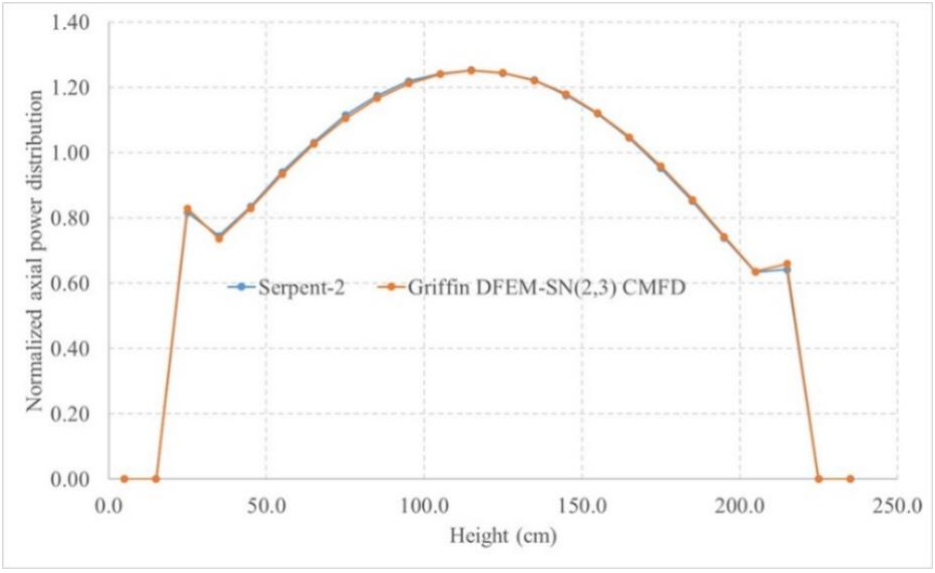

Figure 4-7. Normalized axial power distribution computed by both Serpent-2 and Griffin.

4.3 Preliminary Multiphysics transient modeling of full-core GC-MR

A multiphysic model is established for the full-core GC-MR to capture thermal (temperature) and moderator (hydrogen) effects on neutronics during both normal operation and power transients. The steady state simulation was first performed to predict the operating conditions of the GC-MR design and to provide the initial conditions for any follow up transient simulations. Three types of transient scenarios are investigated. First, a systematic study of the hydrogen leaking effects on reactor performance was conducted, providing insights on how the GC-MR operation is affected by degradation of hydride moderators. Second, a localized single coolant channel blockage transient and a global coolant depressurization transient are simulated.

4.3.1 *Griffin/BISON/SAM/(SWIFT) model development*

The development of the multiphysics GC-MR full-core models, which include Griffin, BISON, SAM (using THM module), and SWIFT, is similar to that of the HP-MR full-core model discussed earlier. The basic hierarchy and single application input files were adopted from the previous multiphysics GC-MR assembly model [5]. The main difference between the HP-MR model and the GC-MR model lies in the grandchild application for heat removal modules: Sockeye for heat-pipes in the HP-MR model and SAM for helium coolant channels in the GC-MR model. Despite the significant differences between the heat-pipe and coolant channel models, their interfaces with the child BISON application remain the same. In the GC-MR model, the channel wall temperature is transferred from BISON to SAM, while the heat flux information (i.e., fluid temperature and heat transfer coefficient) calculated by SAM is transferred back. Although the transfer direction adopted for the GC-MR model is opposite to that used for the HP-MR model, they are equivalent during fixed-point iteration. The selection of either approach is primarily for numerical stability and convergence efficiency.

4.3.2 *Steady-state results*

The Griffin/BISON/SAM/SWIFT model for the GC-MR encountered convergence issues during steady-state simulations. After a few iterations, the residual of the Richardson iteration fluctuated around the 10^{-1} level, preventing the system from reaching a solution. In contrast, the Griffin/BISON/SAM model for the GC-MR, assuming a constant and uniform $YH_{1.94}$ hydrogen stoichiometry, did not exhibit such convergence issues.

It is speculated that the hydrogen redistribution and temperature changes in the system are conflicting with each other (i.e., a change in power density leads to hydrogen feedback and temperature feedback in different directions). This hypothesis is supported by the observation that the Griffin/BISON/SAM/SWIFT system can converge if high-temperature grid points (>925K) are removed from the cross-section, thereby reducing temperature feedback while maintaining hydrogen feedback.

A tentative manual iteration approach was implemented, solving the Griffin-BISON-SAM system with a fixed hydrogen profile calculated based on the temperature from the previous iteration step, to determine the steady-state GC-MR conditions with hydrogen effects. However, this approach is labor-intensive and costly. Further investigations will be made on the convergence issue to reach a fully automated and working Griffin/BISON/SAM/SWIFT model.

The steady-state simulation results of the multiphysics GC-MR model are illustrated in Figure 4-8 and results are summarized in Table 4-2. Note that the SWIFT-involved result was based on five manual iterations with SWIFT as described above, where a relative tolerance in k_{eff} of 2.3×10^{-9} has been reached. Compared to the results shown in Section 3.2.2 for the HP-MR simulation, the GC-MR operates at a higher temperature. Determined by the inlet coolant temperature, the minimum fuel temperature of the GC-MR is around 900 K, the fuel temperature increases along with the axial elevation and reaches 1200 K near the coolant outlet position. As coolant channels are densely distributed, the moderator temperature is comparable with the fuel temperature. Additionally, it is worth noting that the horizontal maximum temperature is not located near the geometric center of the GC-MR. Instead, the horizontal maximum temperature is predicted to be in the middle core region, mainly due to the dissimilar assembly designs in different radial regions.

By involving SWIFT, the predicted hydrogen redistribution was found to lower the reactivity slightly. It is insightful that hydrogen is subjected to additional redistribution if the axial temperature profile changes during transient. Whether such an additional redistribution would lead to positive or negative reactivity feedback would depend on the specific temperature profile changes.

Additionally, while the high effective thermal conductance of heat pipes of the HP-MR results in a small axial temperature difference, the GC-MR exhibits a significant axial temperature difference from the coolant inlet (bottom) to the coolant outlet (top). In the HP-MR, the axial maximum temperature occurs near the reactor midplane due to axial power peaking and the high thermal conductance of heat pipes. Conversely, in the GC-MR, the axial maximum temperature is near the top of the active core region. Consequently, the hydrogen redistribution phenomena in HP-MR and GC-MR differ. Considering the fact that the SWIFT-involved model of HP-MR does not have the similar convergence issue, the difference in hydrogen distribution and its consequent impact on neutronics between the two types of MRs might be the cause of the convergence issue encountered.

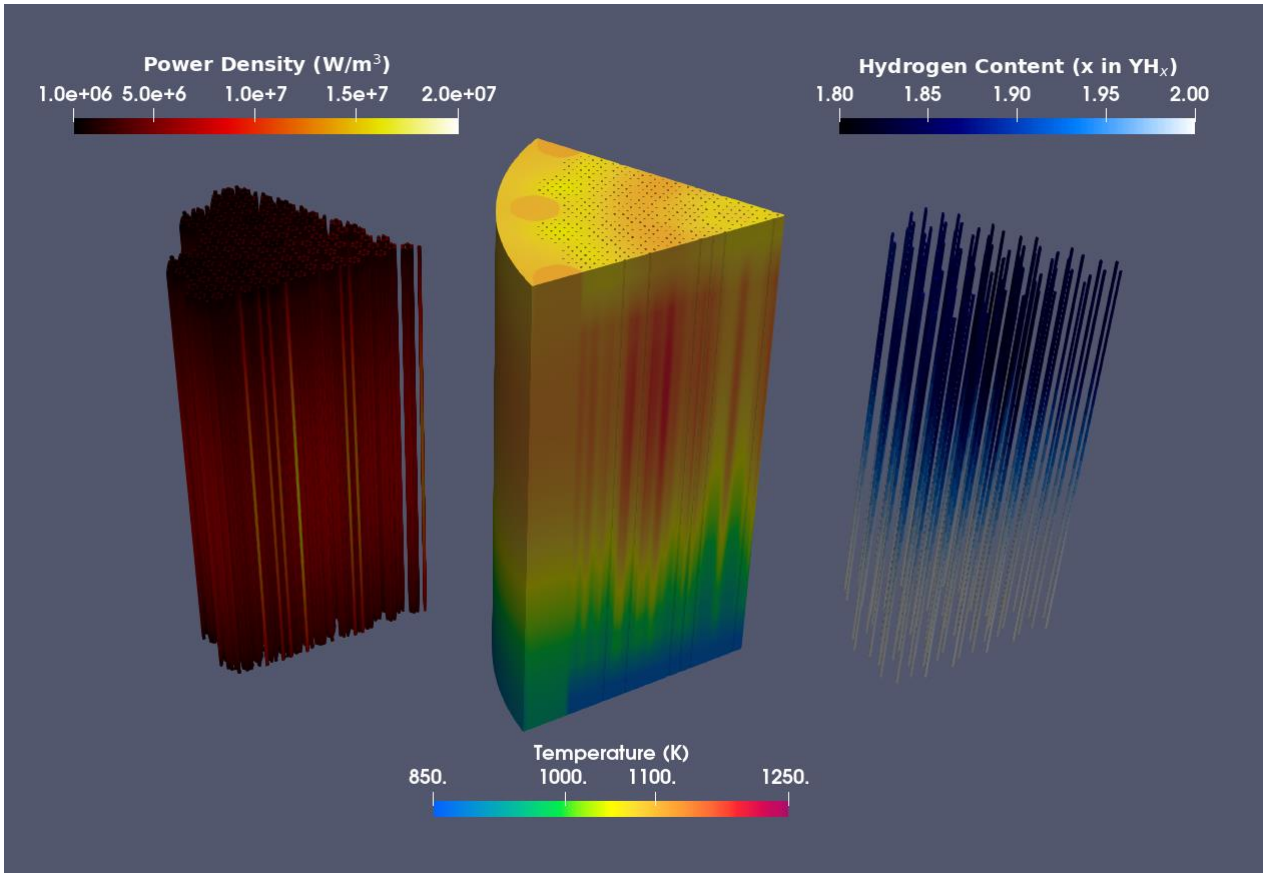

Figure 4-8. Key simulation results of steady-state GC-MR under normal operation condition (five manual iterations with SWIFT results due to the convergence issue).

Table 4-2. Comparison of some key predicted parameters by GC-MR models with and without SWIFT implementation.

Parameter	w/ SWIFT*	w/o SWIFT
Power (MWth)	3.33	3.33
$T_{fuel, avg}$ (K)	1089.85	1088.91
$T_{fuel, max}$ (K)	1210.19	1212.45
$T_{fuel, min}$ (K)	911.08	910.31
$T_{mod, avg}$ (K)	1070.07	1069.14
$T_{mod, max}$ (K)	1173.08	1174.81
$T_{mod, min}$ (K)	912.72	911.93
Keff	1.0289433	1.0292606

* Five manual iterations with SWIFT, due to the convergence issue.

In HP-MR, hydrogen tends to migrate from the midplane to the ends, whereas in GC-MR, hydrogen migrates from the hot top end to the cold lower end. During a loss of heat sink accident, assuming no H_2 leakage, redistributed hydrogen in the moderator tends to migrate back to achieve a nearly uniform distribution as axial temperature differences fade. In such cases, GC-MR and HP-MR may experience different neutronics impacts. As mentioned earlier, hydrogen migration in the moderator has a relatively long relaxation time (kinetics) compared to conventional power transient events. However, if the accident lasts long enough, these effects may still need to be seriously considered. Also, as the GC-MR operates at a higher temperature, the hydrogen kinetics in the GC-MR is also faster than that in the HP-MR.

4.3.3 *Simulations of hydrogen leaking incidents of various severity levels*

Despite the convergence issue mentioned above, comprehensive transient studies based on the Griffin/BISON/SAM/SWIFT are yet possible. As hydrogen leaking incidents dominantly depend on the hydrogen feedback instead of the temperature feedback, the high temperature grid points were artificially removed from the cross-section to enable the convergence of the steady state simulation to allow investigations on the hydrogen leaking incidents.

In addition to the welding leak incident simulated for the HP-MR, more hydrogen leak scenarios were considered for the GC-MR. As previously discussed, the welding leak is slow (termed “slow leak” in this section) and only leads to minor changes in hydrogen content after approximately 10,000 seconds. Therefore, a “fast leak” case was developed to evaluate the corresponding reactor responses. An artificial approach was used to induce this “fast leak.” Specifically, the entire top boundary of the moderator is artificially removed, allowing a zero Dirichlet boundary condition to be assigned for hydrogen partial pressure. The “fast leak” case is applied to either a single moderator module (the “fast leak single” case) or all moderator modules (the “fast leak all” case). The SWIFT results for both fast and slow leaks for one module are illustrated in Figure 4-9. It is clear that the “fast leak,” as the name suggests, leads to more severe hydrogen leakage within a shorter time span. As a result, the “fast leak” incidents induce much faster power drops in the GC-MR (see Figure 4-10.). Although the “fast leak” incident is extreme and very unlikely to occur in reality, these simulations demonstrate the capability of the multiphysics GC-MR model with SWIFT in predicting the impact of hydrogen evolution on microreactor reactivity.

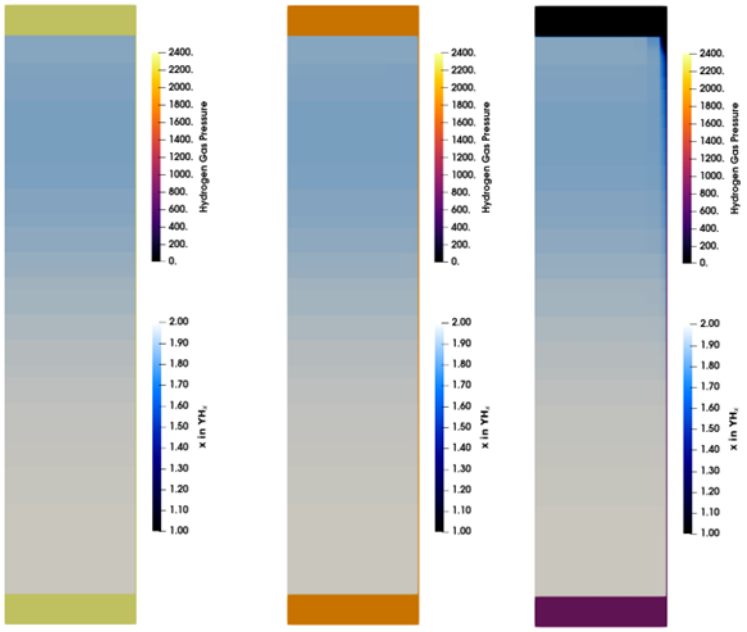

Figure 4-9. Hydrogen distribution in a typical moderator module in the GC-MR: (left) steady state (middle) slow leaking for 2,000 seconds; (right) fast leaking for 200 seconds.

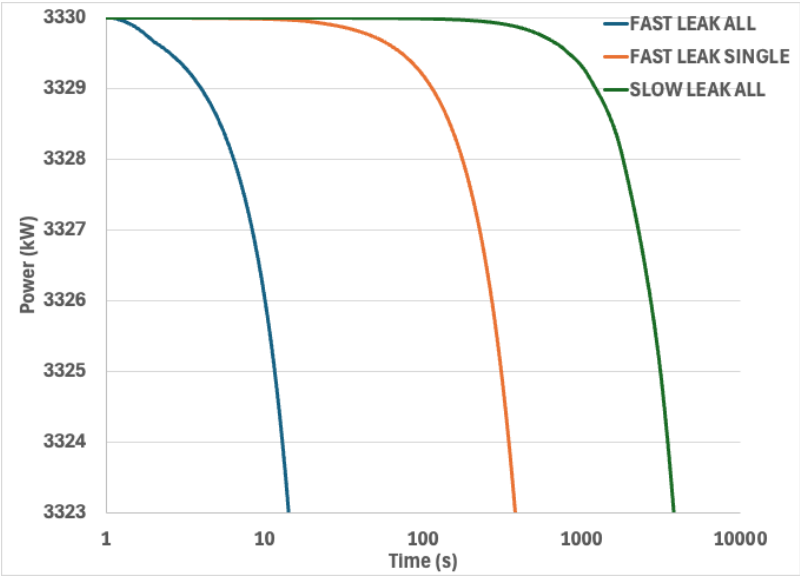

Figure 4-10. Time evolution of GC-MR power during hydrogen leaking incidents of various severity level.

4.3.4 *Single channel blockage transient*

The single coolant channel blockage transient is initiated by setting the coolant velocity of one coolant channel to zero (out of 440 total channels in the 1/6 model of the core). Such a setup effectively eliminates the heat removal capacity of the affected channel. To emphasize the effect of the blockage event, the coolant channel of interest is selected to be in the middle radial region of

the GC-MR where the maximum temperature is observed. As discussed before, the hydrogen migration and leaking has a slower kinetics compared to typical neutronics responses during typical transient scenarios. Therefore, the Griffin/BISON/SAM model without SWIFT was used for this single channel blockage transient simulation, as well as for the coolant depressurization transient simulation to be discussed in Section 4.3.5. The time evolution of the normalized power change is illustrated in Figure 4-11. The power dropped less than approximately 0.5% due to this localized coolant channel event. As indicated by Figure 4-12, the blockage of the single coolant channel near the hottest region of the GC-MR leads to an increase in the maximum fuel temperature by ~28 K. A temperature profile evolution is illustrated in Figure 4-13, highlighting the localized nature of this transient event. In fact, the average fuel temperature is predicted to change by less than 0.1 K throughout the simulation. In summary, with a single coolant channel block, the temperature in the locally affected region slightly increases as nearby channels remove excess heat.

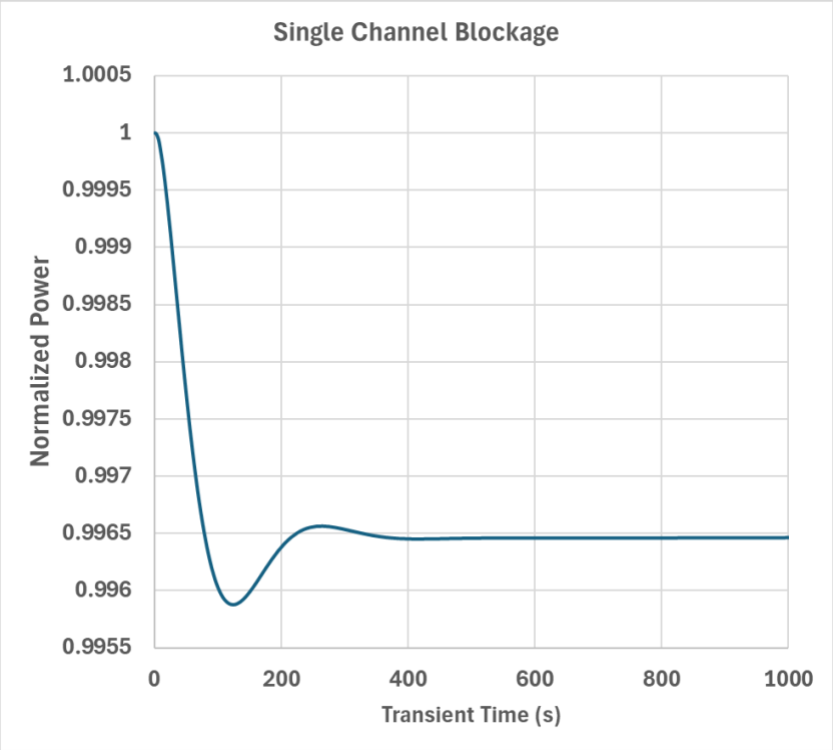

Figure 4-11. Predicted time evolution of normalized power change during a single coolant channel blockage transient.

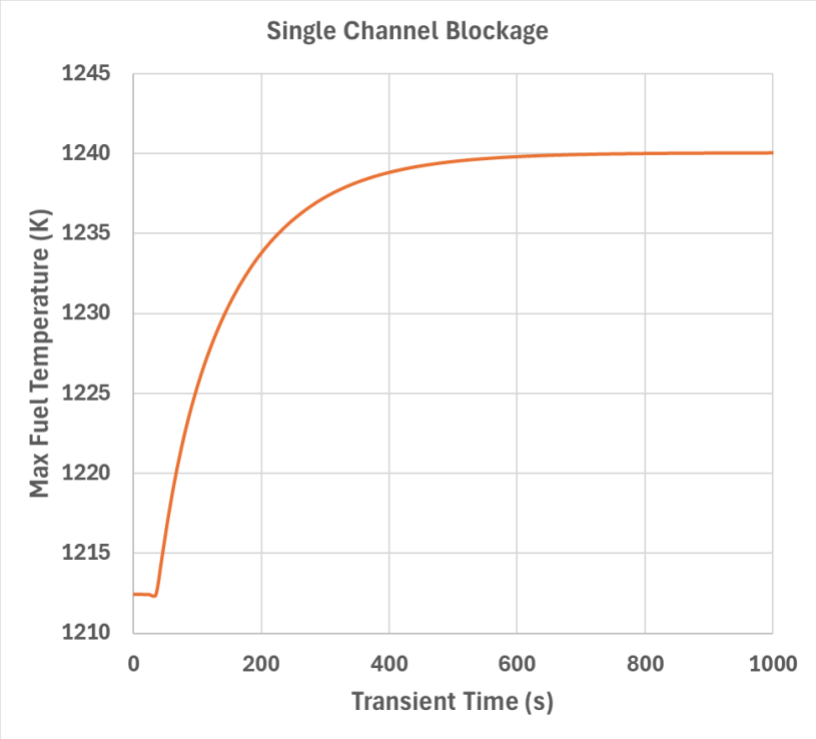

Figure 4-12. Predicted time evolution of maximum fuel temperature change during a single coolant channel blockage transient.

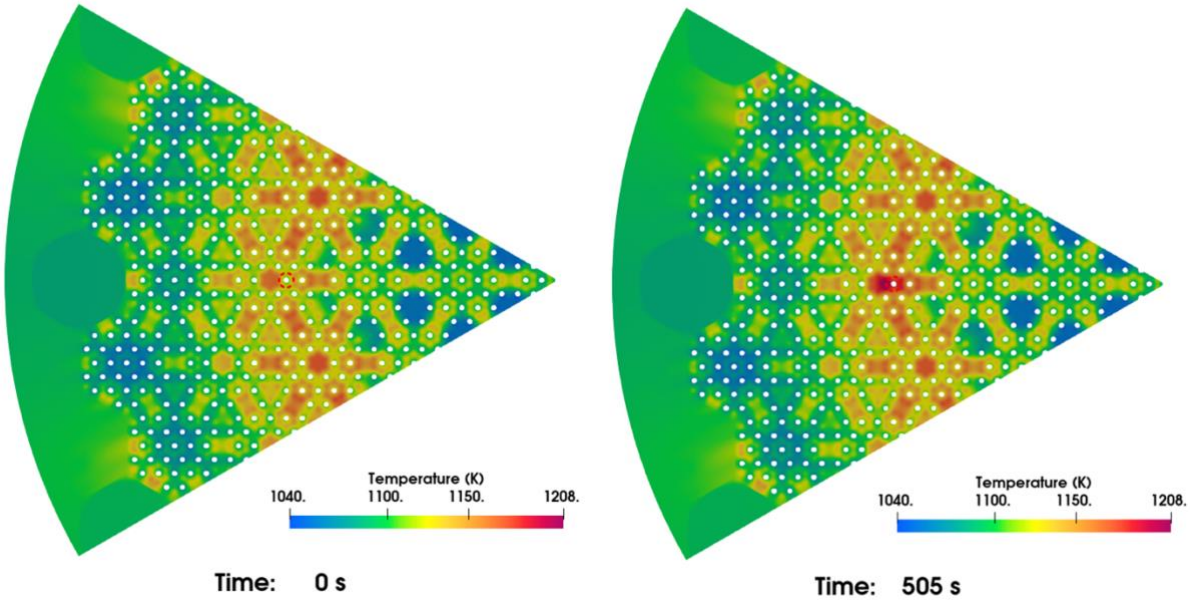

Figure 4-13. The temperature profile changes near the axial midplane of the reactor. The blocked channel is marked by a read circle.

4.3.5 *Coolant depressurization transient*

Compared to the single channel blockage transient, which only has localized effects, the coolant depressurization transient is a global transient event that impact the entire GC-MR core. Within 13

seconds since the initiation of the transient event, the coolant outlet pressure of all the channels drops linearly from 7 MPa to ambient. In the meantime, the velocity of the coolant decreases from 15 m/s to 0.1 m/s. Such an event significantly reduces the global heat removal capacity of the GC-MR and would lead to prominent temperature increase. Similar to the single coolant channel blockage case, the temperature feedback during the high-temperature transient lead to the rapid decrease in reactor power, as shown in Figure 4-14 and Figure 4-15. The GC-MR almost loses all of its original operating power within 400 seconds, along with a maximum temperature increase in fuel by approximately 50 K.

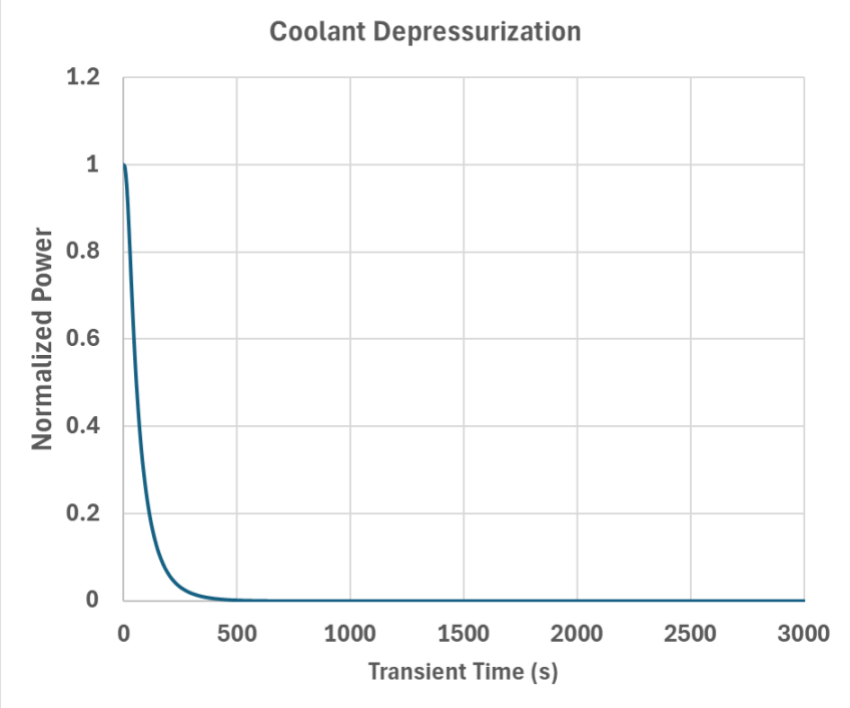

Figure 4-14. Predicted time evolution of normalized power during a coolant depressurization transient.

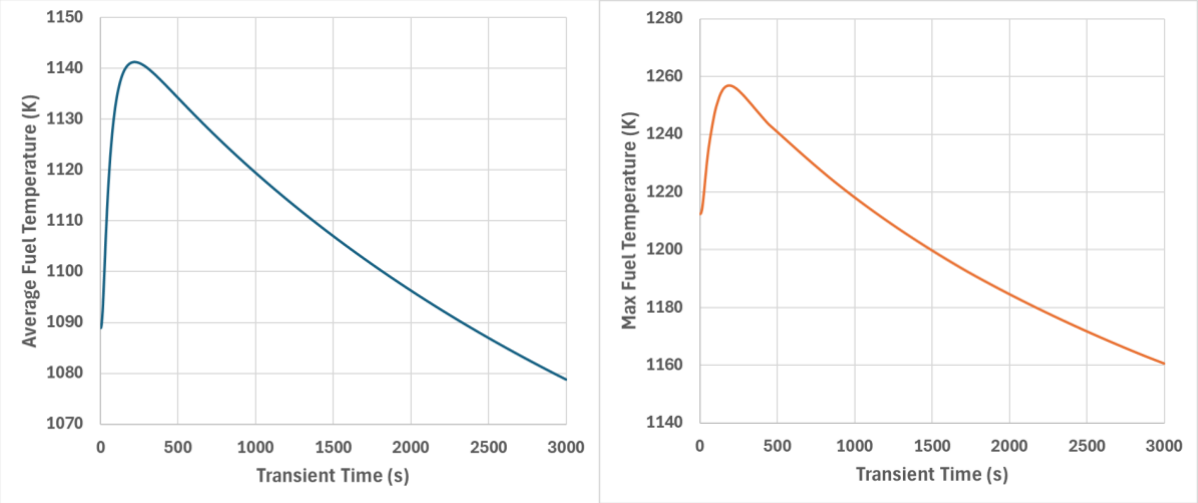

Figure 4-15. Predicted time evolution of average and maximum fuel temperatures during a coolant depressurization transient.

4.4 TRISO failure analysis on the assembly GC-MR

The TRISO fuel performance analysis model for the GC-MR assembly was developed using BISON in FY-2024. We leveraged the coupled Griffin/BISON/SAM Multiphysics GCMR assembly model to generate time-dependent fuel compact power density, temperature, and pressure during a 9.3-year steady-state fuel cycle operation, as well as during reactivity-initiated accident (RIA) and flow blockage transients, introduced in FY-2023 and FY-2022, respectively [5] [4]. Data were extracted from six fuel compacts positioned from the inner center to the outer edge of the assembly at three different heights to capture height-dependent TRISO fuel responses. The updated TRISO model, described in Section 2.3, was employed for these analyses. While the TRISO geometry remains identical, the boundary conditions differ from those in the HP-MR TRISO model. Since the GC-MR is pressurized at 7MPa, the coolant pressure from the SAM code was applied as the external pressure for the TRISO particles. Additionally, like the HP-MR TRISO model, results from the GC-MR full-core Serpent-2 model were utilized to compute the core-average fast neutron flux conversion factor at the beginning-of-cycle, ensuring accurate predictions of fast neutron fluence and corresponding particle deformation.

4.4.1 *Steady-state TRISO failure analysis*

The BISON fuel performance analysis was conducted for TRISO particles located within six fuel compacts at three different heights in the GC-MR assembly. The GC-MR assembly has a 0.1 m radius and consists of 1.6 m long fuel compacts, with 0.2 m long reflectors positioned at the top and bottom of the fuel compacts. Data were extracted from three elevations – 0.25 m, 1.00 m, and 1.75 m – corresponding to the bottom, middle, and top sections of the fuel compact. Figure 4-16 illustrates the power density and temperature distribution of the fuel compact in the GC-MR assembly model at the end of the 9.3-year cycle. The temperature distribution of the fuel compacts appears uniform from the center to the edge of the assembly in the clipped top view at the mid-plane. The axial power profiles predicted by the Multiphysics analysis indicate a shift towards the top of the assembly, resulting in the peak fuel temperature occurring near an elevation of 1.05 m.

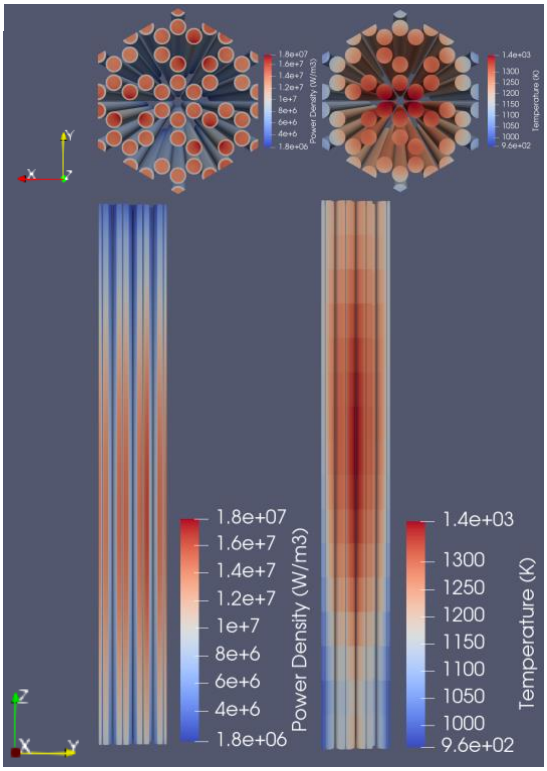

Figure 4-16. Steady-state end-of-cycle fuel compact power density and temperature.

The steady-state TRISO analysis predicted no stress-induced failures but did indicate palladium (Pd) penetration-induced failure in the SiC layer. Palladium, a metallic fission product, is known to accumulate at the IPyC and SiC interface during the irradiation of TRISO particles, where it chemically reacts with the SiC, degrading its structural integrity [21] [22]. The latest BISON Pd penetration model employs an empirical correlation to estimate the rate of Pd ingress into the SiC layer based on the temperature. Failure of the SiC layer occurs when the penetration depth exceeds half its thickness [21]. In the current design, fuel particles located from the center to the bottom of the assembly are prone to SiC failure due to Pd penetration depths exceeding the failure threshold of 17.5 microns, as shown in Figure 4-17 (a). The time to reach the failure penetration depth in the SiC layer can be as early as 5.3 years under high-temperature operation. It is important to note that the current Pd penetration model in BISON is empirical and does not account for factors such as localized attack, Pd concentration, diffusion, and corrosion kinetics. It is notable that Pd penetration-induced failure was not observed in the HP-MR during the 10-year irradiation period, due to the lower fuel compact temperatures compared to the GC-MR. The addition of a zirconium carbide (ZrC) coating layer as a protective layer in TRISO particles has shown to improve resistance to Pd penetration and is an active area of research [22] [23].

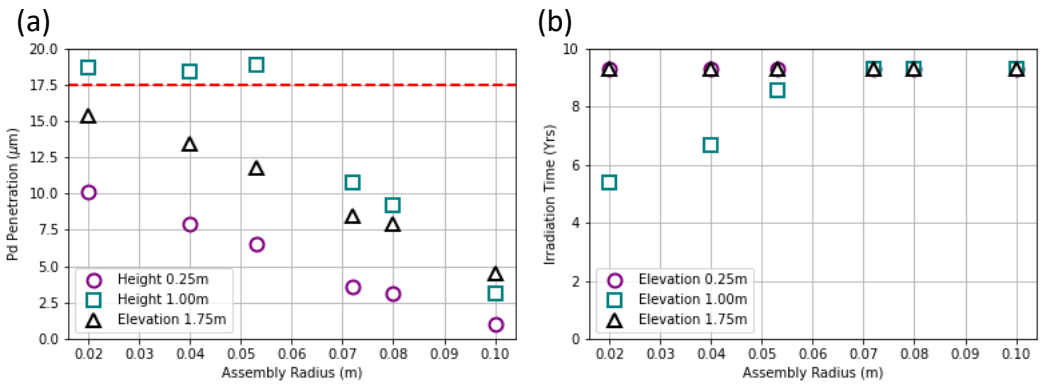

Figure 4-17. Palladium penetration induced failures: (a) penetration depth after 9.3yrs of irradiation and (b) irradiation time reached when Pd failure is achieved.

4.4.2 *Transient TRISO failure analysis*

The Multiphysics modeling of TRISO fuel performance during Reactivity Insertion Accident (RIA) and flow blockage is analyzed to gain insights into fuel behavior under transient conditions (modeled in [5] and [4]) at the end-of-lifetime. Utilizing MOOSE restart capability, one transitioned from 9.3-year steady-state operation to transient scenarios, ensuring continuity in boundary conditions and accurate representation of particle states at the end-of-lifetime. While steady-state analyses identified potential failures due to Pd attack, necessitating the development of a mechanistic Pd corrosion model, transient analyses focused on stress-induced failures by omitting Pd penetration indicators. Results summarized in Figure 4-18 (for RIA) and Figure 4-19 (for flow blockage) demonstrate SiC layer resilience, maintaining a 0% failure rate and compressive stress state throughout both transient scenarios. However, IPyC failure probabilities varied considerably, ranging from 50-65% at the assembly center to 50-100% at the edges. This radial distribution of failure rates correlates strongly with temperature gradients across the assembly. Lower temperatures at assembly edges indicate higher stresses in TRISO particles, primarily due to increased material stiffness, reduced stress relaxation mechanisms, and thermal expansion mismatches between layers. These findings underscore the importance of understanding stress distribution within the TRISO particles and of temperature management in the assembly fuel compacts.

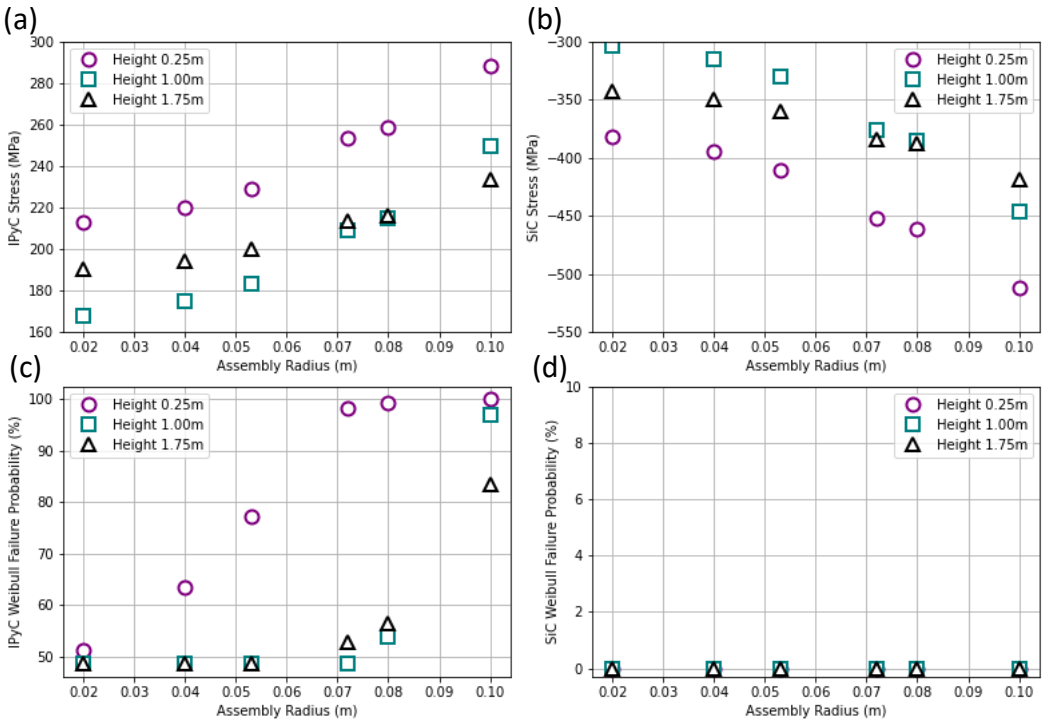

Figure 4-18. RIA transient results: IPyC and SiC layer stress and Weibull failure probability.

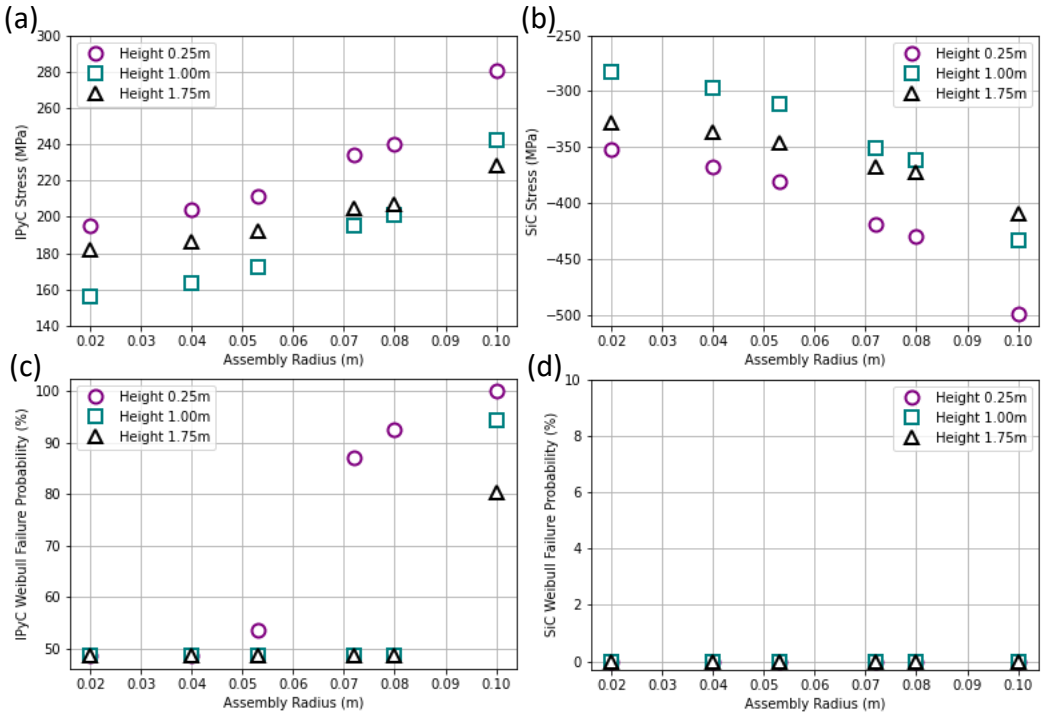

Figure 4-19. Flow blockage transient results: IPyC and SiC layer stress and Weibull failure probability.

4.5 Summary of GC-MR work

Extensive work was completed in FY-2024 on the GC-MR concept with achievements and lessons learned summarized here:

- The full-core GC-MR model was re-design enabling reduced computing time through leveraging core symmetry. The neutronic model was verified through code-to-code comparison showing again satisfactory accuracy obtained with Griffin. It was also released on the INL VTB for use by other programs (such as NRIC) [24].
- Two high-fidelity multiphysics transients were modeled using coupled Griffin/Bison/SAM to simulate moderator leakage (with SWIFT) and flow blockage scenarios. It was noted that the hydrogen kinetics was found to have more impact on the GC-MR with regards to the HP-MR due to higher temperature and larger gradient, leading to convergence issues.
- Additional TRISO failure analyses on the GC-MR assembly model were completed. The amount of SiC failure following accidental transients at end-of-life was null. However, this analysis highlighted Pd penetration rate can be problematic which was activated due to high temperature in GC-MR. This analysis provides guidance into what type of changes in TRISO technology or GC-MR design would be needed to reduce this effect (add coating, reduce temperature or irradiation time, etc.).

5 KRUSTY

The Kilopower Reactor Using Stirling Technology (KRUSTY) was a demonstration of nuclear-powered space reactor jointly funded by the NASA Kilopower Project and the NNSA Criticality Safety Program [25]. The experimental work performed at different testing phases, including cold critical state [26], warm critical state [27], and nuclear system tests [28], provides valuable experimental data for validating numerical codes and models developed under NEAMS projects.

The KRUSTY model was initiated in FY-2022 and was significantly improved through efforts in FY-2023 with a new mesh created using the MOOSE meshing tools and a preliminary multiphysics model for modeling the reactivity insertion transient. In FY-2024, a deep dive on the multigroup cross section generations was completed to improve the accuracy of the Griffin neutronic model. Verification of the Griffin model created for KRUSTY was done by comparing the eigenvalues and axial power distributions to the Serpent-2 results. Validation studies were focused on comparing numerical calculations with experimental data. In particular, in FY-2023, preliminary results were reported on simulating the 15 ¢ reactivity insertion test. In FY-2024, this reactivity insertion test was repeated using the improved neutronic and thermal models. Additional 30 ¢ transient tests were also investigated using the improved multiphysics model.

5.1 Model improvements

Two major improvements have been made for the multiphysics model of KRUSTY. The first one focused on modeling the multi-layer insulation (MLI) layer. The BISON thermal model is tunned such that it can be used to produce a reported thermal equilibrium state [27]. The second one focused on improving the Griffin neutronic model agreement to the Serpent reference model.

5.1.1 *BISON thermal model improvements*

The BISON thermal model has been updated to improve the prediction of warm reactivity insertion transient experiments. The goal was to replicate the experimentally reported thermal behavior of the KRUSTY system used for warm critical experiments (i.e., 30 Wth power leading to 473 K fuel temperature). First, a more careful literature review was conducted to identify more relevant material properties that could be used in the thermal model. A major improvement was the update of the U-Mo heat capacity [29], which is crucial for the fuel temperature prediction during transients. Then, a better approach was adopted for simulating the insulation layer. In the KRUSTY design, a thin insulation layer is used to thermally isolate the fuel from other components to reduce the loss of energy through heat transfer from fuel to reactor external surface. To better simulate the thermal behavior of this thin insulation layer, MOOSE's interface kernel is utilized to model the thermal resistance of the insulation layer without the need to explicitly mesh the thin structure. The thermal resistance of the insulation layer is tuned to match the aforementioned thermal behavior of KRUSTY.

5.1.2 *Neutronics model improvements and verification on the reference core configuration*

In FY-2023, the neutronic analysis showed a large discrepancy by about 1000 pcm on the calculated keff between the Griffin deterministic model and the Serpent-2 Monte Carlo model, when the Griffin model used the multigroup cross sections generated from Serpent-2 [5]. For fast reactors, large discrepancies can result in deterministic calculations if multigroup cross sections are generated from Monte Carlo methods due to the inaccurate scalar flux weighting for the high order

anisotropic scattering cross sections [30]. For this reason, the newly updated MC^2-3 code was used for generating multigroup cross sections.

The MC^2-3 calculation takes two steps to provide multigroup cross sections in ISOTXS format. The first step creates sets of energy self-shielded cross sections for the different reactor core regions over a very fine energy grid (more than 1000 energy groups). These cross sections are imported into an approximated RZ model of KRUSTY as shown in Figure 5-1. Neutron transport calculation was performed by TWODANT [31] to solve the neutron fluxes in each zone of the RZ model. The neutron fluxes from TWODANT includes both the neutron leakage effects and spatial self-shielding effects. In the second step, the neutron fluxes from TWODANT for each region are imported into each MC^2-3 calculation and have been used to condense the cross sections originally on a very fine energy grid to a coarser energy grid provided by the user. For KRUSTY, the same 22-g energy grid used in FY-2023 was used [5]. MC^2-3 can generate both microscopic cross sections for each isotope and macroscopic cross sections homogenized within different regions. In modeling KRUSTY, the zone-averaged macroscopic cross sections were used by Griffin. Currently, MC^2-3 can only work with ENDF/B-VII.0 nuclear library with a beta version of the code updated to work with ENDF/B-VII.1. In our analysis, the ENDF/B-VII.0 version was used.

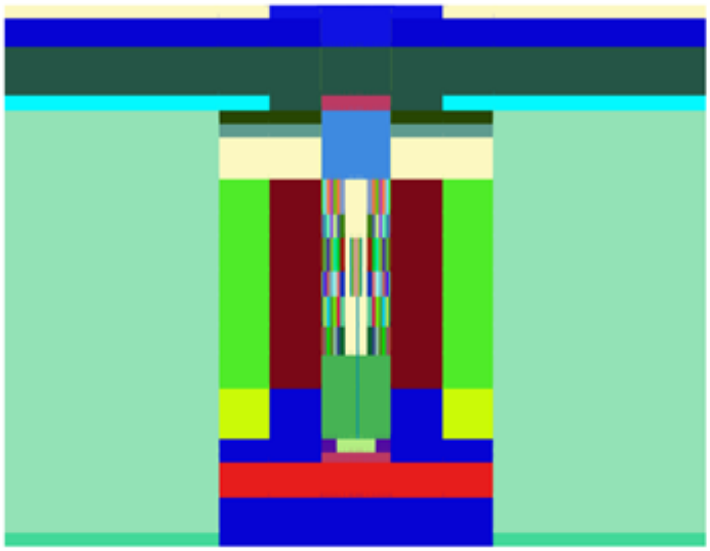

Figure 5-1. KRUSTY RZ model for TWODANT calculation.

Table 5-1 shows the calculated k-effs from Griffin compared with the Serpent-2 reference results. For consistency, the k-effs of using the cross sections from Serpent-2 were also calculated. As shown in the table, large discrepancies are still observed when higher order anisotropic terms were included in Griffin with the Serpent-2 generated cross sections when using the ENDF/B-VII.0 library. However, better agreement is obtained with NA=3 when using MC^2-3 generated cross sections. This exercise confirms that the large discrepancy observed in FY-2023 [5] is due to the inaccurate high order scattering cross sections generated from Serpent-2.

Table 5-1. Calculated k-eff from KRUSTY Griffin models SN(3,5) with different anisotropic order (NA) using Serpent-2 or MC^2-3 generated cross sections and ENDF/B-VII.0 library.

Model	Serpent-2	Griffin + Serpent-2 cross section			Griffin + MC^2-3 cross section		
		NA=1	NA=2	NA=3	NA=1	NA=2	NA=3
keff	1.00267 +/-3pcm	1.00400	1.01476	1.01281	0.99689	1.00951	1.00601
Δkeff [pcm]	Ref.	132	1208	1013	-580	683	334

The results shown in Table 5-1 were obtained from numerical calculations assuming the KRUSTY core is at room temperature (cold state). It demonstrates good agreement among the Griffin neutronic model with the Serpent-2 reference model when the MC^2-3 generated cross sections was used. However, for multiphysics simulation, it is also important to check if the reactivity feedback effects have been correctly modeled as that will determine the reactor dynamic responses. Those results are summarized in Table 5-2. The fuel Doppler reactivity feedback for KRUSTY was evaluated by increasing the fuel temperature from 300 K to 800 K both in the Serpent-2 model and MC^2-3 model. Serpent-2 predicts the keff will be reduced by about 56 ± 2.4 pcm, however, Griffin with MC^2-3 cross sections predicts about 139 pcm reduction in k-eff. This is likely because the Narrow Resonance Approximations used in MC^2-3 may not provide accurate results for KRUSTY due to its thermal tails of the neutron spectrum observed in the thin outer boundary layers.

As shown in FY-2023 report [5], although the Griffin model with the Serpent-2 generated cross sections has large errors in calculating keff, the model captured the fuel Doppler effects accurately with a predicted reduction of about 61 pcm. Therefore, a hybrid cross section set was created for the KRUSTY multiphysics model, which includes MC^2-3 generated cross sections for BeO reflectors where scattering reaction is important and cross sections from Serpent-2 for all other regions. With this hybrid cross section set and NA=3, the difference on k-eff among Griffin and Serpent reference was reduced from 334 pcm to about 220 pcm, and the predicted reduction of keff due to fuel temperature increased to 800 K is 63 pcm, which agrees much better with the Serpent reference value.

Table 5-2. Comparison of the Griffin models with different cross section sets used with Serpent-2 reference model.

Solver XS	Serpent-2	Griffin Serpent-2	Griffin MC^2-3	Griffin Hybrid
K-eff	1.00267 ±3pcm	1.01281	1.00601	1.00488
Doppler [pcm]*	56±2.4	61	139	63

* All Griffin model used scattering term NA=3 and SN(3,5) (NPolar=3 and NAzmthl=5) except that NA=1 and SN(1,3) were used in the model with multigroup cross sections generated from Serpent-2.

5.1.3 *Griffin neutronic model verification on KRUSTY warm critical configuration*

The mesh used in section 5.1.2 modeled four out of KRUSTY's eight heat pipes filled in four of the locations. During the reactivity insertion transient tests, all positions were occupied by steel rods. Therefore, the Griffin neutronics model for multiphysics simulation is slightly different from the standalone neutronics model discussed in Section 5.1.2. Serpent-2 models were also updated accordingly, and a slightly different reference keff was obtained as listed in Table 5-3. The hybrid cross section sets were regenerated for Griffin at different temperature points.

For Griffin to solve the neutron transport equation, spatial variables are discretized by DFEM scheme with shape functions from the first order MONOMIAL family. Angular variables are discretized by the SN method using the Gauss-Chebyshev quadrature. Sensitivity analyses were performed with varying anisotropic scattering terms and with different number of angles used in discretizing the angular space. Table 5-3 compares the keff from all the different Griffin cases to the reference Serpent-2 results. It showed that the calculated keff was converged after using NPolar=3 angles per octant in the polar direction and NAzmthl=5 angles per octant in the azimuthal direction. With scattering term NA=3, the calculated keff from Griffin neutronic model only differs from the reference value by about 223 pcm. Including higher scattering order terms may further improve the accuracy of the neutronic results but will require a lot more computational resource. In the following transient simulation, the neutronic model used NA=3 and SN(2,3) in order to reduce computational time.

Table 5-3. Calculated keff from KRUSTY Griffin models using the hybrid cross sections and with different anisotropic order (NA) and different number of angles.

	Serpent	Griffin (NA=1)					Griffin (NA=2)	Griffin (NA=3)	
		SN(1,3)	SN(2,3)	SN(2,5)	SN(3,5)	SN(3,7)	SN(3,5)	SN(3,5)	SN(2,3)
keff	1.00592	0.99434	0.99750	0.99751	0.99853	0.99854	1.01125	1.00815	1.00703
Δkeff* (pcm)	---	1158	842	841	749	738	-533	-223	-111

*Δkeff =(keff, Serp – keff, Griffin)

The calculated keff at different fuel temperatures are shown in Table 5-4. With the hybrid cross sections, the calculated keff and fuel doppler reactivity feedback by Griffin agree well with the Monte Carlo reference values.

The axial power densities within the fuel region were tallied at cold state and shown in Figure 5-2 a). Compared with the results reported in FY-2023, better agreements were achieved between the Griffin deterministic model and the reference model using the hybrid cross sections. As shown in Figure 5-2 b), the maximum differences were in the outmost boundary layer, where the power production is overestimated by up to 5%. In most of the regions, this difference is within 2%.

Table 5-4. Comparison of the Griffin neutronic results with Monte Carlo reference result using the hybrid cross sections.

	Serpent Reference		Griffin + hybrid XS	
	T_f = 300 K	T_f = 800 K	T_f = 300 K	T_f = 800 K
keff	1.00592 (2 pcm)	1.00513 (2 pcm)	1.00815	1.00752
Δkeff (pcm) ($keff_{Serp}$ – $keff_{Griffin}$)	----	---	-222.6	-229.1
Delta keff (pcm) ($keff_{800K}$ – $keff_{300K}$)	69.0 ± 2.4		62.0	

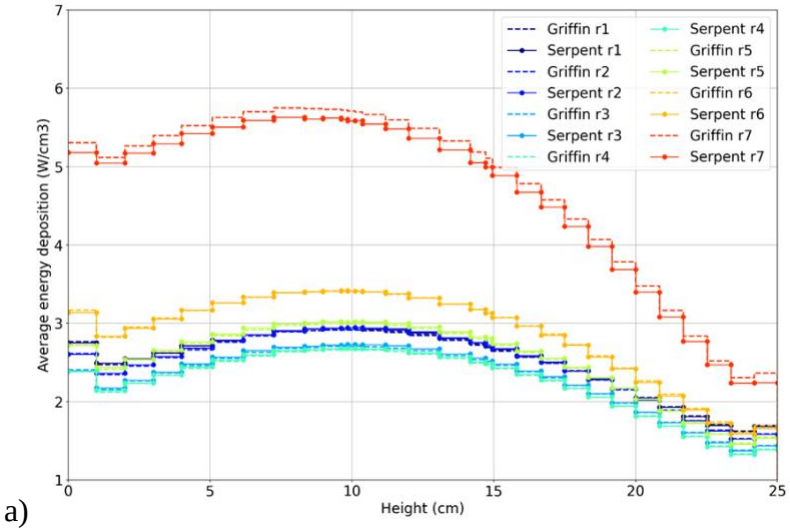

a)

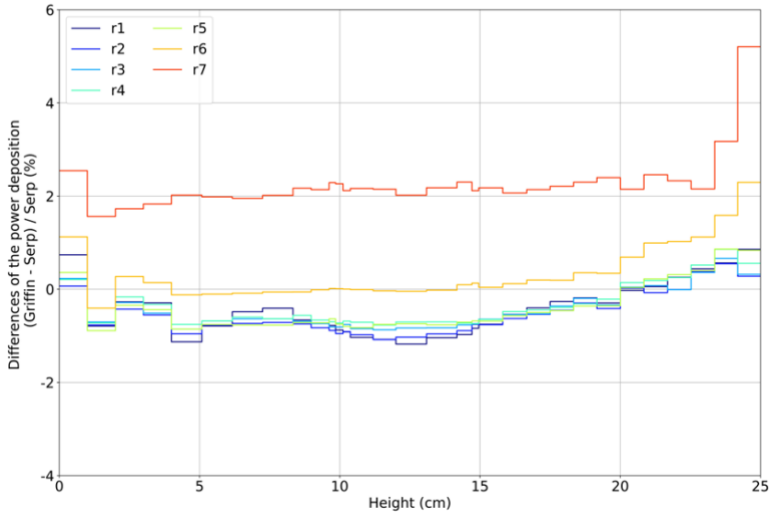

b)

Figure 5-2. a) Calculated fission power deposition in the KRUSTY radial regions b) Differences of the axial fission power deposition (r1: inner first ring of annulus, r7: outermost ring) using the Griffin model (hybrid cross sections) and compared with reference results (solid line: Serpent-2, dash line: Griffin).

5.2 Multiphysics analyses and validation against experimental results

In FY-2024, the updated neutronics and improved thermal models for KRUSTY were integrated to create an enhanced multiphysic model. This model was then used to reproduce the 15¢ reactivity insertion experiment, confirming its superior performance compared to the FY-2023 model. Following this success, the new model was subsequently applied to simulate the 30¢ reactivity insertion experiment.

5.2.1 *Griffin-BISON multiphysics model*

In the KRUSTY warm critical experiments, the power excursion transient was initiated by shifting the radial reflector of KRUSTY upward to insert positive reactivity when the reactor was in a cold/critical state with heat-pipes replaced with solid stainless steel rods. A multiphysics model was prepared to simulate this reactivity insertion test. A two-level MOOSE MultiApps hierarchy was developed, tightly coupling the Griffin neutronics model and the BISON thermo-mechanical model. Griffin, set as the parent (main) application, uses the DFEM-SN(2,3) solver with CMFD acceleration and NA=3 (anisotropic scattering order), while BISON is set as the child application.

The power density profile, initially calculated by Griffin, is transferred to BISON. In BISON, thermo-mechanical computations determine the temperature distribution within all solid components, leading to the calculation of thermal expansion. Both the fuel temperature profile and displacement field are then sent back to Griffin as feedback for the neutronics simulation. The coupling of these two applications occurs through fixed-point iteration. Notably, in this calculation, all heat is passively removed through the external boundary of the reactor, as no heat pipes are involved.

The movement of the axial reflector to insert reactivity was modeled by imposing a Dirichlet boundary condition on the bottom of the solid assembly that includes the axial reflector. This allows BISON to calculate the consequent displacement field by solving solid mechanics equations.

Two steady-state eigenvalue calculations were included to confirm that an adequate amount of external reactivity was introduced for initiating the transient. The first calculation corresponds to the initial steady state for future transient simulation, while the second corresponds to the first step of the transient after the reflector is shifted upward. In this calculation, the bias in the axial direction was set in the BISON input. The displacements were then passed to Griffin neutronics for calculating the total reactivity inserted into the reactor using the MultiApp coupling framework.

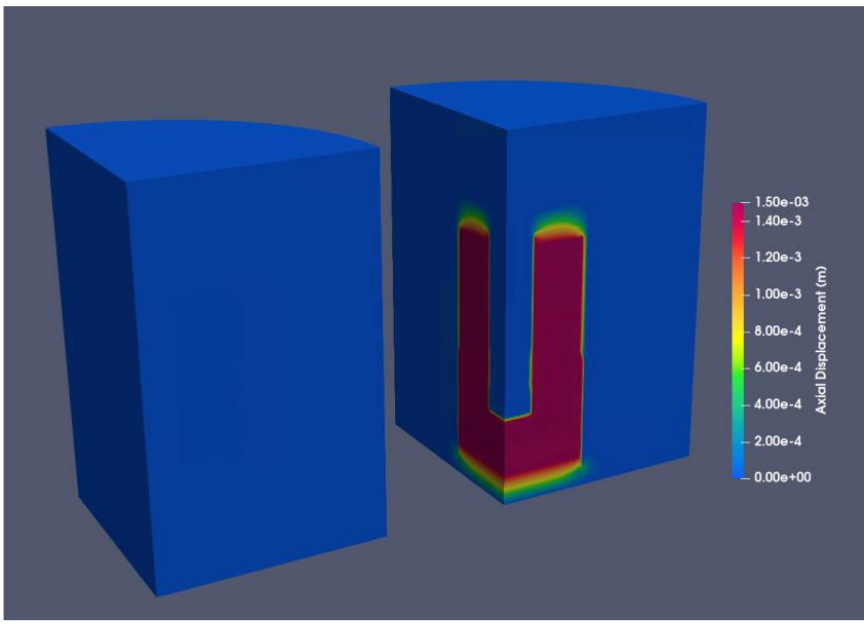

Figure 5-3. Displacement field caused by axial reflector movement to insert reactivity.

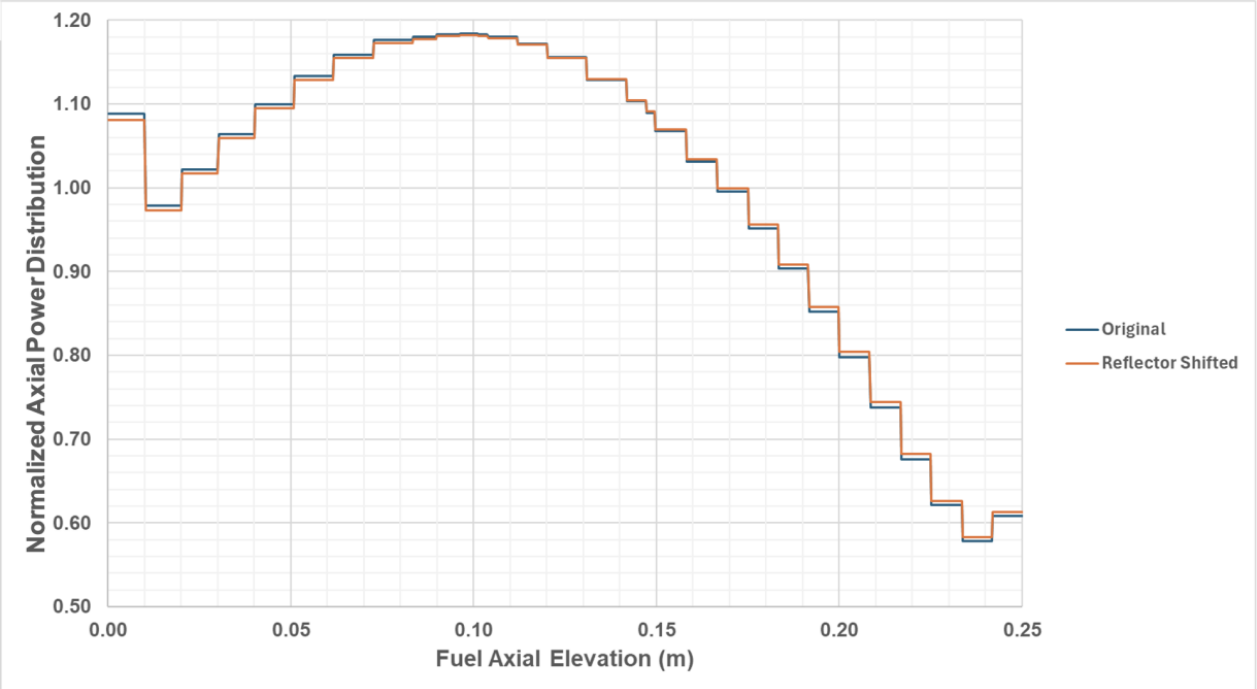

Figure 5-4. The change in power peaking factor before and after the reactivity insertion caused by axial reflector shifting.

The displacement field resulting from the axial reflector movement, as calculated by BISON, is visualized in Figure 5-3. As shown in this figure, applying the 1.48 mm shift boundary condition to the bottom of the axial reflector assembly leads to a uniform shift of the structure, as expected. The keff values before and after applying the axial reflector shift were calculated to be 1.007003 and 1.008008, respectively, using the multiphysics coupled model. This results in an increase of

Δkeff by approximately 100.5 pcm, which is about 14.5 ¢, with a Serpent-calculated βeff of 690 pcm. Figure 5-4 shows the axial power distribution within the fuel disk. The upward shift of the axial reflector also slightly moves the power peaking upward within the KRUSTY fuel region.

5.2.2 *15 cent insertion warm critical test*

In FY-2023, the 15¢ reactivity insertion transient was simulated using the previous neutronics and thermal models. The results showed a consistent trend with the experimentally observed power, though there were some quantitative discrepancies. This transient was rerun using the updated multiphysics model to reduce these discrepancies.

To simulate a 15 ¢ transient event, the power of the ¼ reactor was initially close to zero and artificially set at 0.01 Wth. The transient simulation began from the steady-state result with the radial reflector in its original position. At t=0, the radial reflector was promptly shifted upward by 1.48 mm by altering the axial component of the displacement field variable of the corresponding blocks.

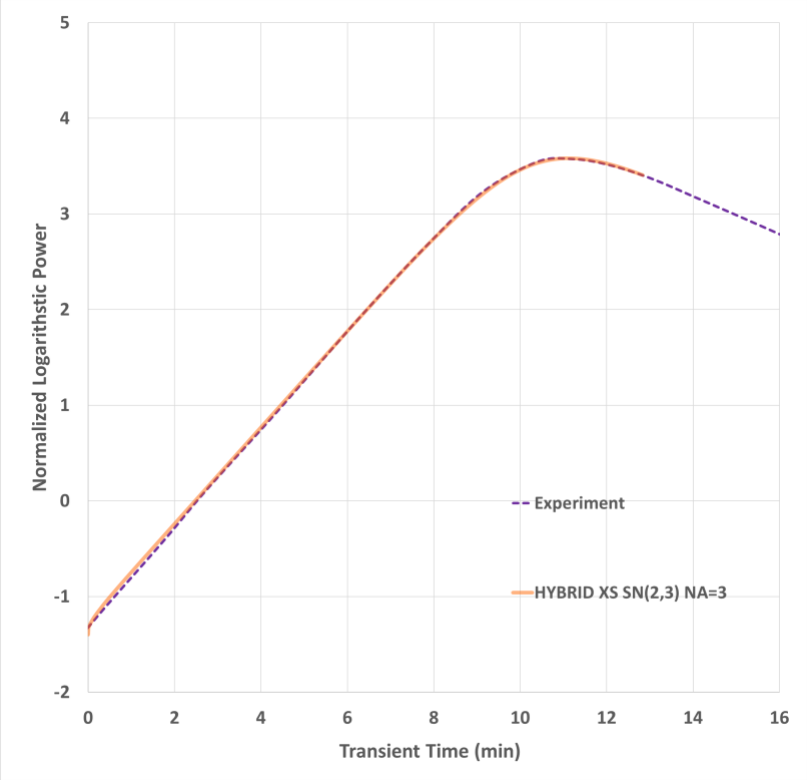

Figure 5-5. Predicted power evolution vs Exp (15 ¢ test)

Due to known bounding issues with the thermocouples and significant uncertainties in the experimental data, only the power evolution results calculated by Griffin were directly compared with the experimental measurements deduced from neutron detector counting, as shown in Figure 5-5. The calculated power ramp-up matches well with the measured values in the initial part of the transient, indicating that the reactivity insertion kinetics are consistent with the experimental specifications. The power ramp-down predicted by the model is also consistent with the experimental observations, suggesting the accuracy of the thermal model. However, the simulated

results show a slightly higher maximum power level (957.4 Wth predicted vs. 937.5 Wth measured for ¼ core), which could be due to a slight insufficiency in temperature feedback compared to the experimental observations.

5.2.3 *30 cent insertion warm critical test*

In this new analysis initiated in FY-2024, the procedure for the 30¢ reactivity insertion transient experiment differs from that of the 15¢ experiment. Instead of a one-time prompt reactivity insertion, the 30¢ transient experiment consists of two distinguishable stages. The first stage involves a prompt 15¢ reactivity insertion, which is technically the same as the standalone 15¢ reactivity insertion experiment. After the power surge introduced by the 15¢ reactivity insertion peaked and dropped back to approximately 3000 Wth (or 750 Wth for the ¼ core model focused on in this report), the second stage of the experiment began. This stage involved gradually moving the reflector so that the remaining 15¢ reactivity was slowly inserted, maintaining the reactor at approximately 3000 Wth for around 150 seconds until the second 15¢ was fully inserted. The reactor power then dropped again.

As the detailed reactivity insertion procedure for the second stage is not available in open literature, assumptions were made to help simulate this stage. After some trials, the 15¢ reactivity inserted in the second stage was equally divided into five pieces (approximately 3¢ each). Each piece of the insertion was made promptly once the ¼ core power dropped below 740 Wth. In this case, the predicted power could be maintained between 740 and approximately 765 Wth for around 130 seconds, as shown in Figure 5-6. Using this modeling approach, simulation results are comparable with the experimental observations. The discrepancies could be reduced or even eliminated if one could reproduce with higher fidelity reactivity insertion procedure used during experiments. The investigators will continue to work on such improvements and are also making efforts to obtain the actual experimental data about the insertion procedure. Another noteworthy phenomenon is that the peak power reported for the first stage of the 15¢ prompt insertion is slightly lower than that of the standalone 15¢ reactivity insertion experiment, which could also be a source of the discrepancies in the second stage.

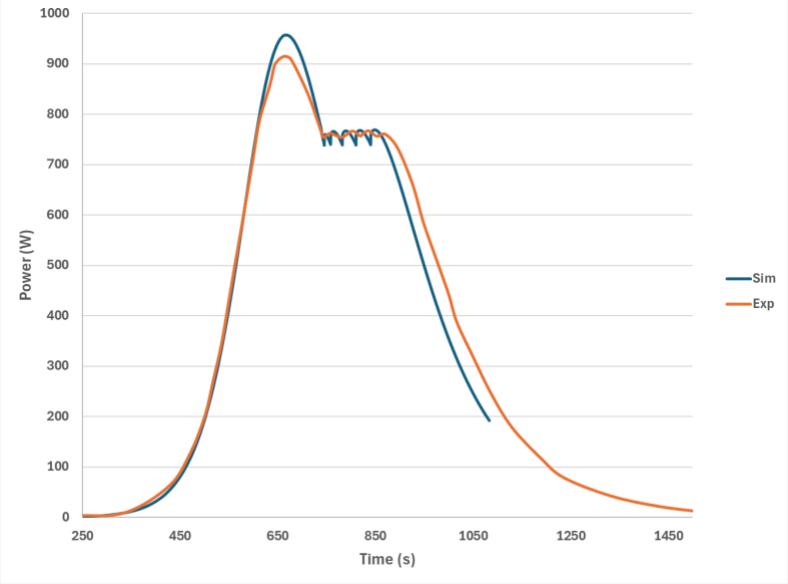

Figure 5-6. Predicted power evolution vs Exp (30-cent test).

5.3 Summary of KRUSTY work

Significant progress was completed in FY-2024 on the KRUSTY modeling effort with the following highlights:

- The neutronics discrepancies observed in FY-2023 were resolved through the use of MC^2-3 and generation of hybrid Monte Carlo/Deterministic set of cross-sections. The resulting neutronic model now provides accurate results through code-to-code comparison. The multiphysics 15¢ insertion transient simulation displayed good agreement when comparing with experimental data.
- Additional transients were modeled with 30¢ reactivity insertion, displaying promising initial results. Improvements are recommended and additional transients will be considered in FY-2025.
- The model developed was released on the VTB [32] and was used for student training at the STARFIRE workshop organized at INL.

6 Summary and Conclusions

Significant progress was accomplished by the team in FY-2024 in further improving multi-physics models of three microreactors systems: HP-MR, GC-MR and KRUSTY. These efforts focused on solving more complex multiphysics problems enabled by enhanced tools capability, verifying and validating results obtained, providing feedback to developers for suggested improvements, and sharing these models to facilitate their wide use for microreactor design and licensing.

6.1 Capability demonstration of micoreactor modeling capability

On the HP-MR, a series of new multiphysics (Griffin/BISON/Sockeye) transients were modeled, with core startup transient, control drum inadvertent rotation accident, and hydrogen leakage (also including SWIFT). The TRISO failure analyses completed in FY-2023 were updated leveraging improved TRISO modeling capabilities that led to higher IPyC failure probability without affecting SiC failures.

On the GC-MR, a new full-core model was developed and analyzed through a series of new multiphysics (Griffin/BISON/SAM) transients to simulate moderator leakage (including SWIFT), depressurization, and flow blockage. Those demonstrated high inherent safety behavior of the GC-MR. Additional TRISO failure analyses on the GC-MR assembly model were completed. The amount of SiC failures following accidental transients at end-of-life was null. However, this analysis highlighted Pd penetration rate can be problematic and may require design changes (add coating, reduce temperature or irradiation time, etc.).

On KRUSTY, the neutronics discrepancies observed in previous years were resolved through the use of hybrid set of Monte Carlo/Deterministic cross-sections. The multiphysics 15¢ insertion transient simulation displayed good agreement when comparing with experimental data. And initial modeling of the 30¢ reactivity insertion also displayed promising results.

This project led to many publications with the objective to share models and communicate progress with end users. The high-fidelity Multiphysics HP-MR model demonstration was published in a journal paper [19]. Four conference papers were published on this project: at the ANS winter 2024 on recent VTB models [33], at PHYSOR on KRUSTY [32], and two papers at the ANS Winter 2023 on FY-2023 work [34, 35].

Three models were published on the VTB, with HP-MR TRISO failure analyses (based on FY-2023) [36], new GC-MR core Griffin model [24], and KRUSTY multiphysics steady-state model [32]. Those VTB models were highlighted by NRIC in a journal paper [37], and two conference papers [38] [39]. In addition, the Sockeye HP-MR unit-cell multiphysics startup tutorial developed in FY-2023 was submitted for integration into the Sockeye code documentation.

6.2 Lessons learned in terms of microreactor multiphysics modeling

Through this work, some valuable experience was gathered in terms of microreactor modeling best practices. The modeling of hydride moderator performance in the multiphysics simulations of the HP-MR and GC-MR showed notable differences. While the coupling of the SWIFT model with other physical models was smooth for the HP-MR, similar approaches for the GC-MR led to convergence issues. It is speculated that the temperature and hydrogen feedback mechanisms might conflict when solved together within the current fixed-point iteration framework. The differences between the HP-MR and GC-MR may stem from their distinct axial temperature profiles, determined by their respective heat removal mechanisms and the resulting hydrogen redistribution

modes. Further investigations are needed to identify the best practices for handling the GC-MR multiphysics model with SWIFT coupling.

The TRISO failure analysis done on the HP-MR and GC-MR highlighted the importance of the improved stress modeling that led to significant increase in IPyC failures observed with regards to the simplified approach used last FY. The very different pressure and temperature conditions in the GC-MR and HP-MR highlighted different failure mechanisms, demonstrating the importance of these types of simulations during core design process. The TRISO analysis from the GC-MR assembly model demonstrated potential SiC failure due to Pd penetration. This finding highlights the need for mechanistic Pd penetration models and corresponding failure criteria. It is important to note that there are additional failure modes beyond those already mentioned, which require further investigation. These include fabrication defects, delamination, outer PyC layer crack, and Ag permeation, among others. These failure modes have not yet been fully addressed in our current analysis. As the TRISO model in BISON continues to improve, we will focus on incorporating these additional failure modes to enhance the comprehensiveness and accuracy of the analysis.

6.3 Support to NEAMS developers

Finally, important experience was gathered with the NEAMS tools leading to several user feedback shared with code developers, especially with regards to MOOSE mesh generator and Griffin. This project made also great stride in further enhancing the verification and validation of NEAMS tools. Additional code-to-code neutronic verification exercises were completed on the HP-MR and GC-MR, complementing previous findings [18] and confirming Griffin accuracy, in particular confirming that the cross-section multi-dimensional interpolation approach utilized in Griffin sufficiently accommodates variations in both temperature and hydrogen content. Furthermore, the close agreement obtained for the KRUSTY multiphysics (Griffin neutronics / BISON thermal-mechanics) transient analyses with experiments provides important validation data that can be leveraged by microreactor vendors to support licensing of their technology.

6.4 Recommended follow-up work

The following additional tasks are recommended to expend on this work:

- Continued V&V activities, including further KRUSTY multiphysics modeling of experimental transients.
- Structural modeling capability of thermomechanical response of graphite monolith in GC-MR or HP-MR is recommended as a new activity.
- Sockeye improved mechanistic modeling should be assed and demonstrated on the HP-MR, to further improve the initial work completed here on startup transients.
- Work completed in FY-2023 with GC-MR balance of plant modeling should be continued by integrating this model into the full-core multiphysics model developed this FY for load following and accidental transient analyses. Modeling of fission products poisoning may also be considered.
- Improvements in TRISO particle neutronic and thermal modeling was identified as potentially important in literature [40] and should be investigated.

- Models developed in FY-2024 needs to be submitted to the VTB, to update past models or provide new capabilities: KRUSTY transient model, updated TRISO failure model, HP-MR control drum rotation, and full-core GC-MR transients analysis.

References

[1] C. R. Stanek, "Overview of DOE-NE NEAMS Program," https://www.osti.gov/biblio/1501761, 2019.

[2] C. Matthews, V. Laboure, M. DeHart, J. Hansel, D. Andrs, Y. Wang, J. Ortensi and R. C. Martineau, "Coupled Multiphysics Simulations of Heat Pipe Microreactors Using DireWolf," *Nuclear Technology,* vol. 207, no. 7, 2021.

[3] N. E. Stauff, K. Mo, Y. Cao, J. Thomas, Y. Miao, L. Zou, E. Shemon, B. Feng, K. Ni and C. Matthews, "Detailed analyses of a TRISO-fueled microreactor," ANL/NEAMS-21/3, September 30, 2021.

[4] N. E. Stauff, A. Abdelhameed, Y. Cao, K. Kristina, Y. Miao, K. Mo and D. Nunez, "Multiphysics Analysis of Load Following and Safety Transients for MicroReactors," ANL/NEAMS-22/1, September 30, 2022.

[5] N. Stauff, A. Abdelhameed, Y. Cao, N. Fassino, L. Ibarra, Y. Miao, K. Mo and D. Nunez, "High-fidelity multiphysics load following and accidental transient modeling of microreactors using NEAMS tools," ANL/NEAMS-23/4, 2023.

[6] Y. Wang, Z. M. Prince, H. Park, O. W. Calvin, N. Choi, Y. S. Jung, S. Schunert, S. Kumar, J. T. Hanophy, V. M. Labouré, C. Lee, J. Ortensi, L. H. Harbour and J. R. Harter, "Griffin: A MOOSE-based reactor physics application for multiphysics simulation of advanced nuclear reactors," *Annals of Nuclear Energy,* vol. 211, 2025.

[7] R. L. Williamson and e. al., "BISON: A Flexible Code for Advanced Simulation of the Performance of Multiple Nuclear Fuel Forms," *Nuclear Technology,* vol. 207, pp. 954-980, 2021.

[8] J. E. Hansel and et al., "Sockeye Theory Manual," INL/EXT-19-54395, March 2020.

[9] H. Hu and et al., "An advanced one-dimensional finite element model for incompressible thermally expandable flow," *Nuclear Technology,* vol. 190, 2015.

[10] C. Matthews, A. Shivprasad and M. Cooper, "Metal Hydride Simulations Using SWIFT," LA-UR-21-27538, July 2021.

[11] A. D. Lindsay, D. R. Gaston, C. J. Permann, J. M. Miller, D. Andrš, A. E. Slaughter, F. Kong, J. Hansel, R. W. Carlsen, C. Icenhour, L. Harbour, G. L. Giudicelli, R. H. Stogner, P. German and e. al, "2.0 - MOOSE: Enabling massively parallel multiphysics simulation," *SoftwareX*, vol. 20, p. 101202, 2022.

[12] E. Shemon, Y. Miao, S. Kumar, K. Mo, Y. S. Jung, A. Oaks, S. Richards, G. Giudicelli, L. Harbour and R. Stogner, "MOOSE Reactor Module: An Open-Source Capability for Meshing Nuclear Reactor Geometries," *Nuclear Science and Engineering*, vol. 197, pp. 1656-1680, 2023.

[13] J. Leppanen, "Serpent – a Continuous-energy Monte Carlo Reactor Physics Burnup Calculation Code, User's Manual," 2015.

[14] C. H. Lee, Y. S. Jung and W. S. Yang, "MC2-3: Multigroup Cross Section Generation Code for Fast Reactor Analysis," ANL/NE-11-41 Rev. 3, 2018.

[15] W. Mueller, J. Blackledge and G. Libowitz, "Metal Hydrides," *Handb. Hydrog. Storage*, 1968.

[16] J. Hansel, "The liquid-conduction, vapor-flow heat pipe model in Sockeye," *Nuclear Engineering and Design*, 2024.

[17] J. E. Hansel, "Sockeye User Documentation," 2020. [Online]. Available: https://sockeye-dev.hpc.inl.gov/site/.

[18] K. Ni, Y. Cao, N. Stauff and J. Hou, "Assessment of griffin cross-section interpolation capability on triso-fueled heat-pipe micro-reactor," in *PHYSOR*, Pittsburgh, 2022.

[19] N. E. Stauff, Y. Miao, Y. Cao, K. Mo, A. A. E. Abdelhameed, L. Ibarra, C. Matthews and E. R. Shemon, "High Fidelity Multiphysics Modeling of a Heat-Pipe Microreactor using BlueCrab," *Nuclear Science and Engineering*, 2024.

[20] Z. Prince and V. Labouré, "Micro Reactor Drum Rotation," NRIC VTB, 2024. [Online]. Available: https://mooseframework.inl.gov/virtual_test_bed/microreactors/drum_rotation/index.html. [Accessed 10 Sept 2024].

[21] D. Petti and e. al, "Development Of Improved Models And Designs For Coated-Particle Gas Reactor Fuels," Idaho National Laboratory, Idaho Falls, ID, 2004.

[22] E. Olivier, J. Neethling and I. van Rooyen, "Investigation of the structure and chemical nature of Pd fission product agglomerations in irradiated TRISO particle SiC," *Journal of Nuclear Materials*, vol. 532, p. 152043, 2020.

[23] T. Ogawa and K. Kukuda, "ZrC coated particle fuel development," in *The Fourth International Symposium on Advanced Nuclear Energy Research*, Japan, 1992.

[24] A. Abdelhameed, Y. Miao and N. Stauff, "Neutronic Modeling of the Whole Core Gas-Cooled Microreactor (GCMR)," VTB, 2024. [Online]. Available: https://mooseframework.inl.gov/virtual_test_bed/microreactors/gcmr/GCMR_Core_Neutronics.html.

[25] D. I. Poston and e. al., "KRUSTY Reactor Design," *Nuclear Technology*, vol. 206, p. S13–S30, 2020.

[26] K. N. Stolte and e. al., "Benchmark of the Kilowatt Reactor Using Stirling TechnologY (KRUSTY) Component Critical Configurations," *Nuclear Technology*, vol. 208, pp. 625-643, 2022.

[27] D. I. Poston and e. al., "Results of the KRUSTY Warm Critical Experiments," *Nuclear Technology*, vol. 206, pp. S78-S88, 2020.

[28] D. I. Poston and e. al., "Results of the KRUSTY Nuclear System Test," *Nuclear Technology*, vol. 206, pp. S89-S117, 2020.

[29] S. Parida, S. Dash, Z. Singh, R. Prasad and V. Venugopal, "Thermodynamic studies on uranium–molybdenum alloys," *Journal of Physics and Chemistry of Solids*, vol. 62, no. 3, 2001.

[30] C. Lin and W. S. Yang, "An assessment of the applicability of multigroup cross sections generated with Monte Carlo method for fast reactor analysis," *Nucl. Eng. and Tech.*, p. 2020.

[31] R. E. Alcouffe, F. W. Brinkley, D. R. Marr and R. D. O'Dell, "User's Guide for TWODANT: A Code Package for Two-Dimensional, Diffusion-Accelerated, Neutral-Particle Transport," LA-10049-M, 1990.

[32] Y. Cao, Y. Miao, K. Mo and N. Stauff, "Kilopower Reactor Using Stirling TechnologY (KRUSTY)," VTB, 2024. [Online]. Available: https://mooseframework.inl.gov/virtual_test_bed/microreactors/KRUSTY/index.html.

[33] N. E. Stauff, Y. Miao, A. Abdelhameed, Y. Cao, K. Mo and E. Shemon, "NEAMS Microreactor Models Submitted to the VTB in 2024" Submitted – 2024.," in *ANS Winter*, 2024.

[34] N. E. Stauff, Y. Miao, A. Abdelhameed, N. Fassino, Y. Cao, K. Mo, L. Ibarra, D. Nunez and E. Shemon, "Recent and Upcoming Microreactor Models Submission in the VTB," in *ANS Winter*, 2023.

[35] N. J. Fassino, Y. Miao, K. Mo and N. E. Stauff, "Failure Analysis of TRISO Fuel in a Heat Pipe Microreactor," in *ANS Winter*, 2023.

[36] Y. Miao, N. Fassino, K. Mo and N. Stauff, "TRISO Failure Analysis Model Description," VTB, 2023. [Online]. Available: https://mooseframework.inl.gov/virtual_test_bed/microreactors/mrad/hpmr_triso_failure/problem_description.html.

[37] L. Giudicelli and e. al., "The Virtual Test Bed (VTB) Repository: A Library of Reference Reactor Models Using NEAMS Tools," *Nuclear Science and Engineering*, 2023.

[38] A. Abou Jaoude and e. al., "Recent Advanced Reactor Multiphysics Model Highlights in the Virtual Test Bed (VTB)," in *PHYSOR*, 2024.

[39] A. Abou Jaoude and e. al., "Status of New Models Hosted on the Virtual Test Bed (VTB) in 2023," in *ANS Winter*, 2023.

[40] M. Eltawila, A. Novak and Y. Miao, "Coupled Multiphysics Modeling of Heat Pipe Microreactors using Cardinal, BISON, and Sockeye," in *PHYSOR* , 2024.

[41] G. Hu and e. al., "Multiphysics Simulations of Heat Pipe Micro Reactor," doi:10.2172/1569948, 2019.

[42] B. Wilkerson, J. Galloway and C. Matthews, "Thermo-Mechanical-Neutronic Considerations for DireWolf Modeling of the KRUSTY Criticality Experiment," LANL report, 2021.

[43] K. N. Smith and e. al., "KRUSTY: Beryllium-Oxide and Stainless-Steel Reflected Cylinder of HEU Metal," HEU-MET-FAST-101, Nuclear Energy Agency/OECD, 2019.

[44] C.-S. Lin and W. S. Yang, "An assessment of the applicability of multigroup cross sections generated with Monte Carlo method for fast reactor analysis," *Nuclear Engineering and Technology*, vol. 52, no. 12, pp. 2733-2742, 2020.

[45] B. T. Rearden, R. A. Lefebvre, A. B. Thompson, B. R. Langley and N. Stauff, "Introduction to the Nuclear Energy Advanced Modeling and Simulation Workbench," in *M&C* , Jiju Island, South Korea, 2017.

[46] "VTB - HP-MR," ANL, INL, 2023. [Online]. Available: https://mooseframework.inl.gov/virtual_test_bed/microreactors/mrad/index.html.

[47] "VTB - GC-MR," ANL, INL, 2023. [Online]. Available: https://mooseframework.inl.gov/virtual_test_bed/microreactors/gcmr/index.html.

[48] E. Shemon and e. al, "Development and Porting of Nuclear Reactor Computational Models for the NRIC Virtual Test Bed in FY23," ANL/NSE-23/51, 2023.

[49] N. Roskoff and e. al., "Transient analysis of a micro-reactor using the DireWolf code suite," in *PHYSOR 2022*, Pittsburgh, 2022.

[50] A. Abou-Jaoude and e. al., "Status of New Models Hosted on the Virtual Test Bed (VTB) in 2023," in *ANS Winter*, Washington DC, 2023.

[51] N. E. Stauff and e. al., "Recent and Upcoming Microreactor Models Submission in the VTB," in *ANS Winter 2023*, Washington DC, 2023.

[52] N. E. Stauff and e. al., "Applications of NEAMS Codes for Multiphysics Modeling of Several Microreactors Problems," in *ANS Winter 2022*, Phoenix, AZ, 2022.

[53] OECD/NEA, "NEA Benchmark of the Modular High-Temperature Gas-Cooled Reactor-350 MW Core Design: Volumes I and II," NEA/NSC/R(2017)4, 2018.

[54] R. Martin, "Compilation of Fuel Performance and Fission Product Transport Models and Database for MHTGR Design," Oak Ridge National Laboratory, Oak Ridge, TN, 1993.

[55] D. I. Poston, M. A. Gibson, R. G. Sanchez and P. R. McClure, "Results of the KRUSTY Nuclear System Test," *Nuclear Technology*, vol. 206:sup1, pp. S89-S117, 2020.

[56] W. Jiang and e. al., "Efficient Failure Probability Calculations and Modeling Interface Debonding in TRISO Particles with BISON," Idaho National Laboratory, Idaho Falls, ID, 2021.

[57] W. Jiang and e. al, "TRISO particle fuel performance and failure analysis with BISON,," *Journal of Nuclear Materials*, vol. 548, p. 152795, 2021.

[58] A. E. Slaughter and e. al., "MOOSE Stochastic Tools: A module for performing parallel, memory-efficient in situ stochastic simulations,," *SoftwareX*, vol. 22, p. 101345, 2023.

[59] MOOSE, "Brayton Cycle Modeling Guide," [Online]. Available: https://mooseframework.inl.gov/modules/thermal_hydraulics/modeling_guide/. [Accessed September 2023].

[60] A. Moisseytsev and C. Filippone, "Load Following Analysis of the Holos-Quad Micro Reactor,," in *ANS Winter*, Washington DC, 2021.

[61] A. Abdelhameed and e. al., "High-Fidelity Multiphysics Modeling of Load Following for 3-D Gas-Cooled Microreactor Assembly using NEAMS Codes," in *ANS Winter 2022*, Phoenix, AZ, 2022.

[62] C. Lee and e. al., "High Fidelity Multiphysics Simulation of Holos Quad Micro Reactor Design,," in *ANS Winter 2022*, Phoenix, AZ, 2022.

[63] R. A. Lefebvre, B. R. Langley, L. P. Miller, M. Baird and B. S. Collins, "NEAMS Workbench MOOSE Integration Update," ORNL-TM-2021-2141, 2021.

[64] D. I. Poston, "Data and Insights for the KRUSTY Nuclear-Powered Tests," LA-UR-21-26141, 2021.

Nuclear Science and Engineering Division
Argonne National Laboratory
9700 South Cass Avenue, Bldg. 208
Argonne, IL 60439

www.anl.gov

Argonne National Laboratory is a U.S. Department of Energy laboratory managed by UChicago Argonne, LLC